IVM Institute for Environmental Studies

An Assessment of the Impacts of Climate Change on Coastal Inundation on Bonaire

Job Dullaart

Stan van Manen

Report R-22/05
28 September 2022

This report is released by: Pieter van Beukering
Director Institute for Environmental Studies,
Vrije Universiteit Amsterdam

This report was commissioned by: Greenpeace Nederland

IVM
Institute for Environmental Studies
Vrije Universiteit Amsterdam
De Boelelaan 1111
1081 HV AMSTERDAM
The Netherlands
T +31-20-598 9555
E info.ivm@vu.nl

Greenpeace Nederland
NDSM-Plein 32
1033 WB Amsterdam
The Netherlands

Contents

Summary

Bonaire is as a small and low-lying island state vulnerable to the impacts of climate change. In the future decades, sea level rise and tropical cyclones are expected to increase coastal flood risk on the island. Yet, it is still unknown to what extent coastal flooding will increase and which areas on Bonaire are expected to flood. Therefore, this study aims to assess the impacts of climate change on coastal inundation on Bonaire. First, a static bathtub model is used to estimate the future coastlines of the island under multiple sea level rise projections. Second, the SFINCS model is applied to incorporate the dynamic storm components of storm tide and waves in addition to sea level rise. The results of the inundation models indicate that coastal inundation becomes critical for large parts of Kralendijk in 2150 under scenarios SSP5-8.5 and SSP5-8.5 LC. Under the more optimistic scenarios SSP1-2.6 and SSP2-4.5 coastal inundation remains limited to the nature reserves of Klein Bonaire, Lac Bay and the saliñas. Therefore, the results of this study indicate the importance for Bonaire of globally limiting climate change to a lower-end future climate scenario.

1 Introduction

Small island states in the Caribbean are one of the most vulnerable places in the world to climate change (Nurse *et al.*, 2014; Taylor *et al.*, 2018). Sea level rise (SLR), tropical cyclones (TCs) and shifting rainfall patterns are, amongst others, climate-related drivers of future flood risk for smaller islands. Consequently, this is expected to have large negative socioeconomic implications on sectors including agriculture, fisheries, tourism, freshwater resources, financial facilities, human settlements and health (Nurse *et al.*, 2014).

Bonaire is part of the Dutch Antilles in the Caribbean. As a small island state, it is considered to be exposed to climate change (Nurse *et al.*, 2014). Large parts of the island, including the capital Kralendijk, are only up to a few meters above sea level; making Bonaire particularly prone to SLR, TCs, and surges (Petit & Prudent, 2008). Over the last three decades, Bonaire has been affected by several TCs, e.g., TCs Lenny (1999), Ivan (2004) and Omar (2008) caused construction damages, coastal erosion and large coral bleaching events (Schmutz *et al.*, 2017; Scheffers & Scheffers, 2006; Steneck *et al.*, 2019). SLR, as well as the growing population, are only expected to increase coastal flood risk on the island (Verweij *et al.*, 2020). A future with increased coastal flood risk will not only cause economical losses, but it will also affect Bonaire's cultural heritage, public health and marine ecosystems (De Boer, 2022; Baertz, 2022; Van der Knaap).

To better assess future coastal flood risk on Bonaire, it is important to get a clearer understanding of the inundation events. With the modern-day coastal inundation models, it is possible to dynamically simulate coastal flood events in an accurate and computationally efficient way (Leijnse *et al.*, 2021). While certain models have been applied in many coastal locations in the world (Sebastian *et al.*, 2021; Athif, 2020; Leijnse *et al.*, 2021), dynamic coastal inundation models have not been applied on Bonaire until now.

Therefore, the aim of this study is to evaluate coastal flooding on Bonaire under different climate scenarios. First, the future coastlines of Bonaire will be assessed, using different SLR projections ranging from 2050 till 2300. Then, the impact of storm events on coastal inundation will be evaluated by dynamically incorporating storm tide and waves into a coastal inundation model. Lastly, the influence of coral reef degradation on inundation extent will be assessed.

1.1 Research objective

The main objective of this research is to answer the following question: "How does climate change impact coastal flooding on Bonaire?"

This main research question will be assessed with the use of the following sub-questions:

- How will SLR affect permanent inundation on Bonaire?
- How will storm events impact coastal flooding on Bonaire under different climate scenarios?
- How will the coral reef state impact coastal flooding on Bonaire?

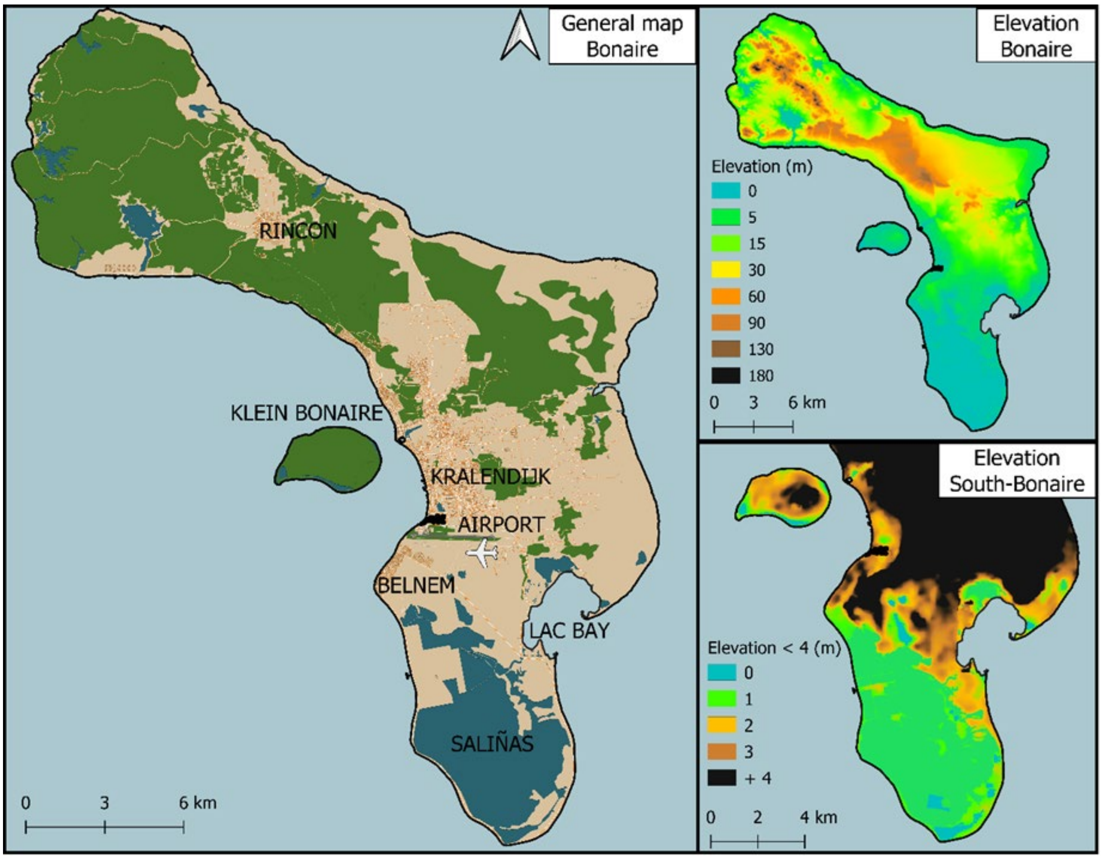

Figure 1 a) General map of Bonaire including low-lying areas vulnerable to coastal flooding; b) Elevation map of Bonaire; c) Elevation of south-Bonaire with focus on elevation < 4m

1.2 Introducing Bonaire and its climate

Bonaire is a Caribbean island, part of Leeward Islands in the Dutch Antilles. Since the Netherlands Antilles dissolved in 2010, Bonaire became a special municipality of the Netherlands. The island is 288 km2 and has a rapidly growing population, with almost 22.000 inhabitants in 2021 (Statistics Netherlands, 2021). The economy of Bonaire is largely dependent on tourism, with roughly 500.000 tourists a year (Van der Lely *et al.*, 2013). Kralendijk is the main port and capital of Bonaire, located on the west coast of the island (Figure 1a).

Compared to the two other special municipalities of the Netherlands, Bonaire is relatively flat. Especially the south of the island, including the saliñas, is low in elevation (Figure 1c). The saliñas are habitat for a unique biodiversity, including the Antillean flamingo (Figure 2a), but it is also economically used for salt harvesting (Verweij *et al.*, 2020). Other important low-lying ecosystems are Lac Bay and Klein Bonaire. Lac Bay is a lagoon with large mangrove forests (Figure 2b) and Klein Bonaire is a small offshore island with large reefs around the island. Both ecosystems are home to the sea and green turtle, among other species, making both locations valuable ecosystems (Verweij *et al.*, 2020; Van der Lely *et al.*, 2013). Besides valuable ecosystems, also urban areas are located on the flat parts of the island. Kralendijk itself is located directly on the coast and partly on low-lying land, while the same goes for the neighbourhood of Belnem, south of Kralendijk and the airport (Figure 1).

Figure 2 Photos of the permanently inundated nature reserves, saliñas (left) and mangroves of Lac Bay (right) Photo credit: Sophie Buijs

1.2.1 Current climate on Bonaire

Bonaire's climate is classified as an arid steppe climate with a distinguished wet and dry season. The island is located in the southern Caribbean dry zone, where precipitation is characterised by its extreme annual variability. From February until May the dry season runs on the island, while the rain season is running from October until January. During the rainy season, showers can be expected in the early morning or in the evening. August and September are considered transition months towards the rainy season. Additionally, from June until the end of November the hurricane season runs on the island. Bonaire is located at the southern boundary of the Atlantic hurricane region, causing the amount of passed hurricanes, within a radius of 150km, to be limited to once every four years (Meteorological Department of Curaçao, 2016).

The average temperatures on Bonaire range seasonally from 26 to 29°C, with the highest mean temperatures in September. The ocean average temperature lies around 27°C and is warmest from September until October and coldest from February until March, with a temperature of 28.2°C and 25.9°C respectively. Furthermore, Bonaire's northern and eastern shores are subjected to persistent easterly trade winds with substantial wave energy, whereas the southern and western coasts mostly have calm low-energy wave conditions (Meteorological Department of Curaçao, 2016; Schmutz *et al.*, 2017).

1.2.2 Climate change on Bonaire

Over the last decades, the climate on Bonaire has changed (KNMI, 2021). Due to the lack of multi-year accurate time series of temperature on Bonaire, the KNMI (2021) estimated the past temperature trend of Bonaire using time series of Curaçao. In the European Netherlands, multi-year temperature trends have been available from the early 20th century for multiple locations. Since the 1980s, the KNMI observed an annual average temperature increase of 0.15°C per decade on Curaçao, which is a total increase of 0.6°C until today. For precipitation neither a positive nor a negative trend has been found on the island since 1960 (KNMI, 2021). Moreover, climate change on the Caribbean islands is expected to increase in intensity in the coming decades (IPCC, 2021). The Climate Studies Group Mona (2020) analysed regional climate models that simulated temperature and precipitation patterns up to the year 2100. For all climate scenarios temperature is expected to increase, ranging from 0.83 to 3.05°C (Table 1). Furthermore, annual precipitation is expected to decrease for all climate scenarios as well, ranging from -0.09% to -16.95% (Table 2).

In addition, 14 TCs with windspeeds over 18m/s within a radius of 250km of Bonaire have been recorded since 1981 (KNMI, 2021). Due to the low frequency of TCs this time-series is too short to observe a trend. As a result, calculating RPs of extreme winds and elevated sea levels based on this data might lead to an over- or underestimation of the actual probability. Yet, within the North Atlantic region, which includes Bonaire, a 17% increase in frequency of intense TCs has been recorded since 1990 (Stephenson & Jones, 2017). Despite this positive trend, it remains a challenge to identify long term trends of storms and TCs due to the lack of homogeneous historical instrumental data. Therefore, the Intergovernmental Panel on Climate Change (IPCC) states a low-confidence in long term trends in both TC intensity and frequency (Seneviratne *et al.*, 2021). To obtain future TC projections, the World Meteorological Organization (Knutsen *et al.*, 2020) and the United Nations (Cha *et al.*, 2020), both requested a confidence assessment on TCs, with similar and consistent conclusions. Most high-resolution global climate models predict considerable reductions in the total number of TCs as the climate warms, with the majority of the reductions occurring towards the weaker end of the intensity spectrum (low-to-medium confidence interval). On the other end of the spectrum, the frequency of the intense 4-5 category TCs is expected to increase globally (medium confidence interval). Furthermore, the intensity of TCs and the precipitation rate are projected to increase globally as well (medium-to-high confidence interval). Overall, the total number of TCs is expected to decrease while the number of major TCs (> category 3) is expected to increase.

Table 1 Projected annual temperature change for 2050 and 2100 under 3 SSP scenarios (The Climate Studies Group Mona, 2020)

Temperature°C	2050	2100
SSP1/RCP2.6	0.86°C	0.83°C
SSP3/RCP6.0	1.00°C	1.85°C
SSP5/RCP8.5	1.50°C	3.05°C

Table 2 Projected annual precipitation change for 2050 and 2100 under 3 SSP scenarios (The Climate Studies Group Mona, 2020)

Annual precipitation change	2050	2100
SSP1/RCP2.6	-0.09	-0.46
SSP3/RCP6.0	-4.30	-5.26
SSP5/RCP8.5	-6.27	-16.95

2 Theoretical framework

To define the most relevant concepts related to the scope of this research, a theoretical framework is provided in the following section. Literature assessing the theories associated to coastal inundation modelling and water level forcing will be discussed to provide a scientific background to this study. This chapter will elaborate on static and dynamic inundation modelling, SLR, storm tide (ST) and wave set-up (WSU).

2.1 Static and dynamic inundation modelling

Compound Coastal inundation modelling knows three different simulation approaches: the simple, reduced-physics and full-physics modelling approach. Within those approaches there is a trade-off between accuracy and computational power, described in Figure 3 by Leijnse et al, (2021). Simple flood models demand minimal computational power, but at the costs of limited accuracy. On the other hand, full-physics process-based models demand high computational power, but can accurately simulate flooding. In the middle of this trade-off relation, reduced-physics models aim to produce an as high as possible accuracy at an as low as possible computational demand (Leijnse *et al.*, 2021). Due to this delicate balance between accuracy and computational demand, the type of coastal inundation model should be dependent on the goal of the research. As the goal of this study is twofold, both a static and a reduced-physics model will be used.

Firstly, a static model is used to determine which areas will become permanently inundated under future SLR scenarios. Thereafter, a reduced-physics model is used to simulate coastal flood inundation under storm events, including forcings such as SLR, ST and WSU. The static model will be referred to as the bathtub model, while the reduced-physics model is called Super-Fast Inundation of CoastS (SFINCS). In the methods section there will be an elaboration on the approaches and techniques of both models.

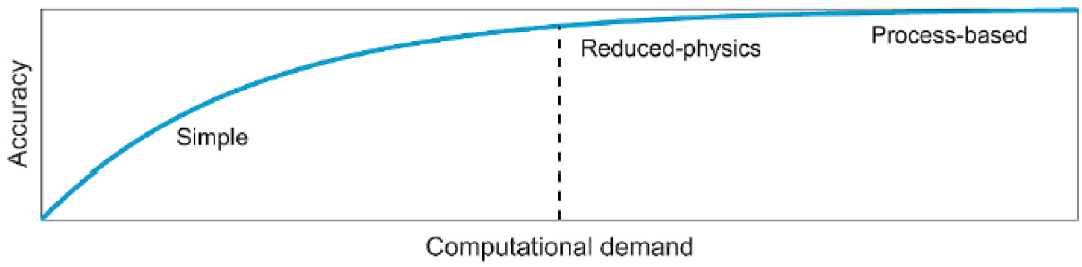

Figure 3 Conceptual figure describing the relation between accuracy (y-axis) and computational demand (x-axis) for the three modelling approaches of inundation models (Leijnse et al., 2021)

2.2 Water level forcing

As the main purpose of this study is to accurately model inundation under multiple climate scenarios, it is important to understand the varying water level forcing that are applied as input in the models. Figure 4 illustrates the three types of water level forcing: 1) SLR, 2) ST and 3) WSU, of which the latter is affected by coral reefs. To better understand these processes, the theoretical background behind all forcing types will be discussed in the following section. Here, a literature review will be given, while later in the methodology, the actual data collection of all forcing types will be explained.

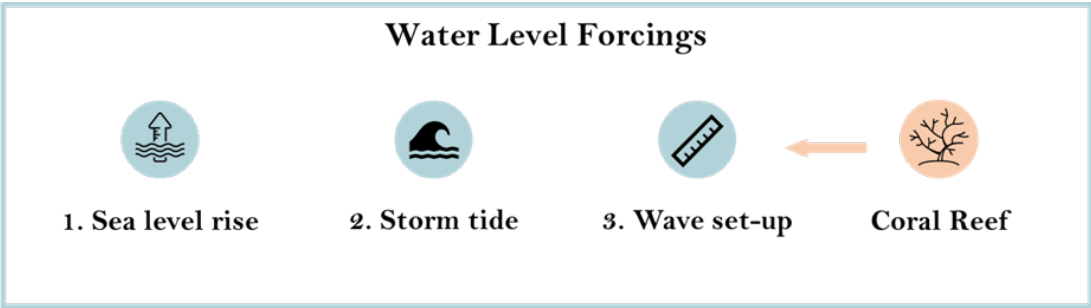

Figure 4 Conceptual figure of the three modelled water level forcing components and the effect of coral reef on wave set-up

2.2.1 Sea level rise

SLR is the increase in the oceans water level relative to a reference point in time. The latest IPCC report (AR6) estimated the global mean sea level (GMSL) to have risen between 0.15-0.25m over the period 1901-2018, with an accelerated rise since the end of the 1960s (Fox-Kemper *et al.*, 2021). The total sea level change is a contribution of 5 different SLR-drivers separated by the IPCC: Thermal expansion, the change in glacier volume (excluding Greenland and Antarctica), change of the Greenland ice sheet, change of the Antarctic ice sheet and the change in land-water storage (Oppenheimer *et al.*, 2019). Currently, the contribution of each component to the GMSL change is 38.4%, 40.8%, 24.5%, 4.1% and -7.8% respectively. However, it is important to note that the confidence level of each component varies. For example, the estimated land-water storage contribution to GMSL change has a low confidence level, while thermal expansion has a medium confidence (Fox-Kemper *et al.*, 2021).

Thus, the GMSL changes are mainly driven by thermal expansion and the melting of land ice. Nevertheless, local sea levels are also influenced by other physical mechanisms causing the redistribution of water around the world. Among those physical mechanisms are the heterogeneity of the earth’s gravitational field and its rotation speed (Le Bars *et al.*, 2019). Due to these geophysical and gravitational forces, the Caribbean is expected to see a larger SLR compared to the GMSL changes (Simpson *et al.*, 2011).

Current studies on SLR in the Caribbean Sea show similar sea level trends compared to the global SLR. However, due to the lack of long historical sea level records in the Caribbean, there is a higher uncertainty in sea level trends compared to studies on global sea level trends (Climate Studies Group Mona, 2020). Sea level trends have been estimated with both satellite observations and gauge stations by two studies with similar results. Palanisamy *et al.*, (2012) estimated the SLR in the Caribbean to be 1.8 mm/year for the period 1950 to 2009, while a similar rate of 1.7 mm/year is calculated by Torres and Tsimplis (2013) over the period 1993 to 2010. These rates are similar to the global rate of 1.7mm/year during the same time period (IPCC, 2013).

The IPCC (2021) established climate models that project SLR on a global scale with regional deviations. In future projections of SLR, the estimated change is very much dependent on how climate and society is going to change. To incorporate both physical and socioeconomic factors into SLR scenarios, the IPCC follows the so-called Shared Socioeconomic Pathway (SSP) – Representative Concentration Pathway (RCP) framework (Van Vuuren & Carter, 2014; O'Neill *et al.*, 2020). SSPs are descriptions of how society may evolve up to the year 2100 and follow societal factors concerning demographics, economic growth, governance and human development. In total, there are five different SSPs to cover a range of possible societal futures. Next to the SSPs, RCPs are more related to the physical change in climate. RCPs are defined as descriptions of how climate may evolve over the rest of the 21st century in a quantitative way. They project future atmospheric concentrations of greenhouse gases and the climate changes they will cause (O'Neill *et al.*, 2020).

In the latest SLR projections of the IPCC, five of these scenarios are used to cover a range of possible future development of anthropogenic drivers. All scenarios start in 2015 and go until the end of this century. In this study, three of the five scenarios are used to model future inundation on Bonaire. To simulate a wide range of possible futures for Bonaire, it is chosen to model low-end, medium and high-end scenarios of the IPCC. These chosen scenarios are SSP1-2.6, SSP2-4.5 and SSP5-8.5 and correspond to an estimated global mean surface temperature warming at the end of the 21st century of 1.8, 2.7 and 4.4°C respectively. This is relative to pre-industrial global mean temperatures (IPCC, 2021). Besides the three SSP scenarios, an extra high-end scenario is modelled: SSP5-8.5 Low Confidence (LC). This is the same climate scenario as SSP5-8.5, however, the modelled SLR projections of this scenario include uncertain melting processes of the Greenland and Antarctic ice sheets (IPCC, 2021). Due to the inclusion of those ice sheet processes, the deviation in the SLR projection models is large for the SSP5-8.5 LC scenario. Nevertheless, the mean projected SLR in this scenario is the highest compared to the other three modelled scenarios.

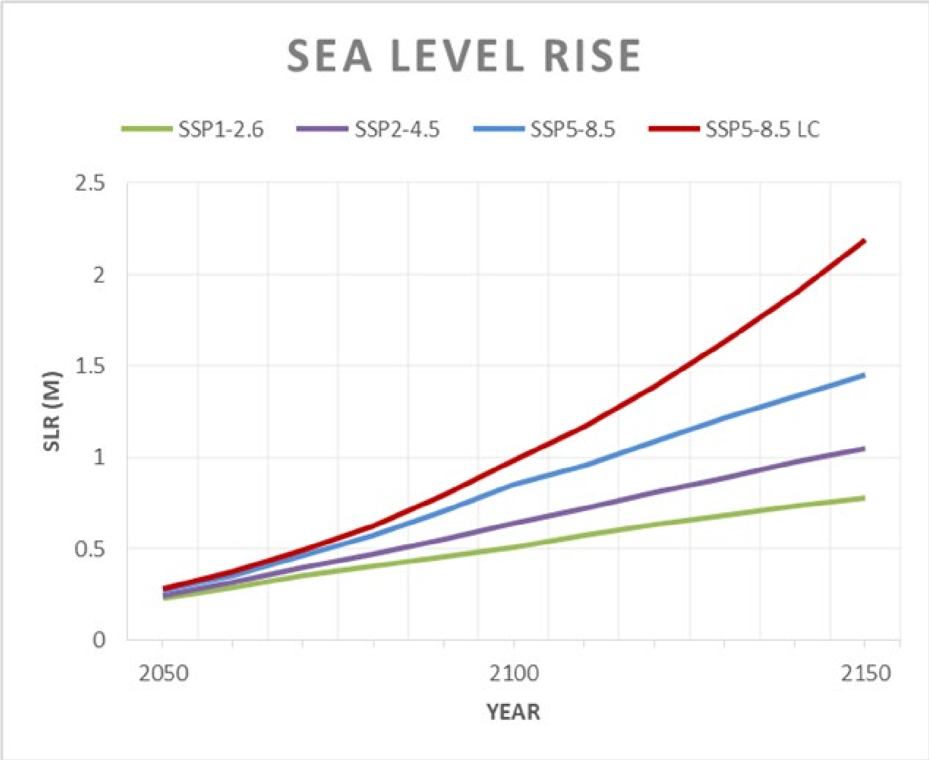

Figure 5 IPCC (2021) SLR projections of the four modelled SSP scenarios up to the year 2150

Most SSP SLR projections in this study will be simulated up to the year 2150. Figure 5 depicts the mean projected SLR for all modelled scenarios. In 2050, the differences between the scenarios is only a few centimetres, while in 2150 the scenarios range from 0.78-2.19m of SLR (NASA, 2022; IPCC, 2021). In addition to the simulations up to 2150, two scenarios will be modelled for the year 2300. The IPCC (2021) incorporated two SLR projections for low-end scenario SSP1-2.6 and high-end scenario SSP5-8.5 for 2300. Both scenarios report a low confidence level, because they both include the uncertain Greenland and Antarctic ice sheet processes. The 17th-83rd percentile projections range from 0.6-1.5m for SSP1-2.6 LC and 2.2-5.9m for scenario SSP5-8.5 LC, indicating the high uncertainty of the SLR estimations in the far future. In this study, the mean SLR projections of 1.05 and 4.05m respectively are modelled.

2.2.2 Storm tide

Storm tide is defined as the combination of two components: storm surge and tide. Storm surge is the increase of the water level caused by the forcing from atmospheric disturbances and its length can vary from a few minutes to a few days (Danard *et al.*, 2003). Storm surge is considered the most damaging component of TCs and Extra Tropical Cyclones (ECTs) (Harley, 2017). While the potentially stronger winds in TCs can result in higher storm surge levels, ETCs occur more frequently and generally affect a larger coastal area. The tidal component in the ST is the height of the oscillation of the ocean surface twice a day, caused by the Earth’s gravitational attraction of the sun and moon (Myers, 1975). The height of the tide differs globally, where the tidal range is generally smaller in the open ocean compared to shallow continental shelves (Pugh, 2004).

On Bonaire, ST has a relatively low contribution to the total water level. Dullaart et al, (2021) modelled global ST levels and showed that both tide and storm surge are small compared to other locations in the world. The Caribbean sea is known for its micro-tidal range, with a mean tidal range of less than 20cm (Torres & Tsimplis, 2011). Van Zee (2022) reports the tidal ranges around Lac Bay on Bonaire. A larger tidal range between 27.1 and 28.1 cm was found on open water, while in the bay itself the tide ranges from 3.4 to 8.1cm. According to this small tidal amplitude, lower extreme sea levels can be expected on Bonaire. Muis et al, (2016) conducted a global reanalysis of storm surge and extreme sea levels and found that relatively high extreme sea levels occur at locations with high tidal amplitudes. Furthermore, storm surge on Bonaire is dependent on the bathymetry around the island. Because of its steep continental shelf and relatively deep ocean, water masses are larger and storm surge cannot develop well. This makes the effect of storm surge minor compared to coasts with shallow shores, bays or oceans where storm surge can grow more easily (Weaver & Slinn, 2010).

In this study, only the ST level of the 1 in 100-year extreme events will be used in the scenario analysis. The difference between the 1 in 100-year ST and the 1 in 1000-year ST is approximately 20cm around Bonaire (Dullaart *et al.*, 2021). This difference is relatively small compared to the different SLR scenarios, with projections up to 2.04m SLR (IPCC, 2021). Therefore, it is considered more interesting to simulate more different SLR scenarios.

2.2.3 Wave set-up and coral reefs

Wave formation is a very dynamic and complex matter, caused by the water's motion, gravitational forces and wind. As a simplification, it can be divided into three sections from open ocean towards the shore. First, the offshore wave development, where waves are generated by both wind and swell in the deeper parts of the ocean. Then, there is the WSU more towards the shallower coast. It is defined by Guza & Thornton (1981) as the elevation of the mean water level due to the breaking of incident waves coming from the open ocean. The incoming waves from the ocean break towards the shallows, causing the water level to rise, starting the WSU. Observations of laboratory studies report a magnitude of about 10-20% of the incident wave height coming from the open ocean (Kim *et al.*, 2010). The last part in the chain is the wave runup. This can be defined as the maximum water level in the foreshore, caused by the WSU (Guza & Thornton, 1981).

In the dynamic inundation model SFINCS, the processes of wave dynamics will be simplified. WSU will be calculated from the significant wave height of wind and swell, while wave runup will be neglected to simplify the model. Further explanation on the actual calculations on wave height can be read in the methodology section 3.4.

As the process of WSU starts at the shallower waters, the presence of reefs also affects the set up (Tait, 1972; Massel & Gourlay, 2000). The interaction between the reef and the incident waves starts at depths of 50 metres, causing the waves to lose energy (Lugo-Fernández & Roberts, 2011). Additionally, Péquignet *et al.* (2014) reports that swell waves of 2-4 metres dissipate to waves smaller than a metre due to breaking on the outer reef. This is in line with the analyses by Ferraio *et al.* (2014), which concludes an 86% wave energy reduction with the presence of coral reef crests.

Consequently, coral reefs can be seen as an effective protection against elevated WSU. However, climate change is affecting coral reefs, mainly through SLR, warming oceans and ocean acidification, causing coral reef degradation (Wilkinson, 1996; Hoegh-Guldberg, 2011). The degradation has a substantial impact on roughness of the reef, but also on the reef height. Therefore, the WSU could potentially increase in height due to climate change (Ferraio *et al.*, 2014). To simulate the protective characteristic of coral reefs, an extra scenario will be modelled with an increased WSU, replicating the absence of a healthy reef.

3 Methodology

In this part of the study, the various approaches applied to carry out this research are described. An overview of the methodology is illustrated in Figure 6. Centred in this figure are the two coastal inundation models. In this study, the static bathtub model was used to simulate the future coastlines of Bonaire, with SLR as the only water level forcing input variable. With the dynamic SFINCS model the future coastal flood hazards were simulated, including the temporal flow dynamics of ST, WSU and SLR. Besides this water level forcing input data, another important input for inundation models is the Digital Elevation Model (DEM). This DEM was validated with both field measurements and a comparison with another global DEM. Furthermore, the effect of coral degradation on WSU, and therefore inundation, was analysed. Lastly, the results of all climate change scenarios, the DEM validation and the coral degradation simulation were evaluated in the inundation scenario analysis.

This methodology section will start with the used approaches of the input parameters. Then, an explanation will be given on how the two models are applied, followed by the methods of the DEM validation and the coral reef simulation. Lastly, an overview of the modelled scenario is given along with the description of the inundation scenario analysis.

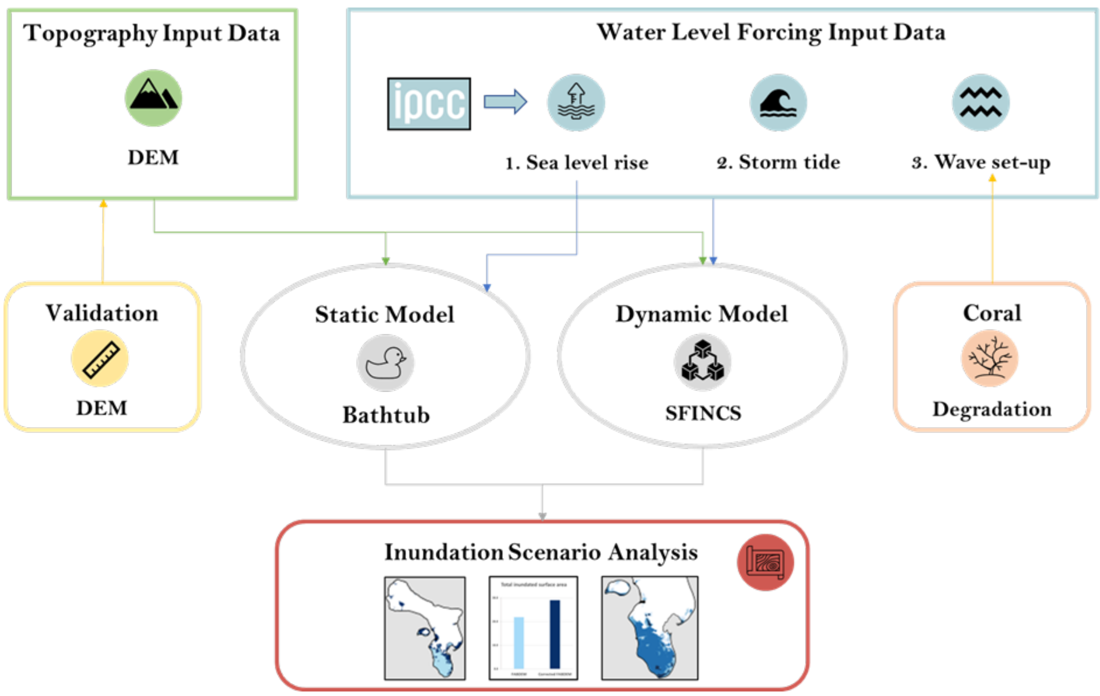

Figure 6 Flowchart representing the methodology of this study

3.1 Model input data

The two models that simulate inundation on Bonaire require both topographic and water level forcing inputs. Here, the methods of input parameters needed for the models will be discussed. This will start with the water level forcing of SLR, which is the only water level input needed for the static model. Next, the dynamic water levels of ST and WSU is explained. Lastly, the most important topographic input data, the DEM, is described.

3.1.1 Sea level rise

To account for the effect of climate change on coastal inundation, SLR is an important input for both inundation models. SLR projections for Bonaire are retrieved from the Sea Level Projection Tool of the National Aeronautics and Space Administration (NASA, 2022). This tool projects global SLR from 2020 to 2150, according to the SSP scenarios of the AR6 IPCC report (IPCC, 2021). For every SSP SLR projection, the quantile is taken as SLR value modelled in this study. The following spatial, temporal and scenario selection of the projection tool were used:

- Scenarios for the years 2050, 2100 and 2150: SSP1-2.6, SSP2-4.5, SSP5-8.5 and SSP5-8.5 LC
- SSP scenarios for the year 2300: SSP1-2.6 LC and SSP5-8.5 LC
- Spatially, the projections of the grid cell where Bonaire is located on is taken: 12°-13°N; 68°-69°W.

Table 3 indicates the projected SLR for all time periods. Additionally, it also summarises the scenarios that were modelled in both inundation models.

Table 3 Estimated values of SLR used in the model simulations of the used SSP scenarios and temporal scales (IPCC, 2021)

SLR (m)	SSP1-2.6	SSP-4.5	SSP5-8.5	SSP5- 8.5 LC	SSP1-2.6 LC
2050	0.24	0.25	0.27	0.28	NA
2100	0.51	0.64	0.85	0.98	NA
2150	0.78	1.05	1.45	2.19	NA
2300	NA	NA	NA	4.05	1.05

3.1.2 Storm tide

ST is a relevant water level forcing when the effect of storms on coastal inundation is modelled. In this study, ST data was retrieved from the COastal dAtaset of Storm Tide Return Periods (COAST-RP) dataset (Dullaart *et al.*, 2021). This is a global dataset with ST levels corresponding to ten different return periods (RPs), ranging from 1 up to 1000 years. For the ST data of TCs, the STORM model by Bloemendaal et al, (2020) was applied to 38 years of global historical TC data from IBTrACS, to statistically extend this dataset to 10,000 years of TC activity. Subsequently, the synthetic tracks from the STORM dataset were used as forcing for the hydrodynamic Global Tide and Surge Model (GTSM) to simulate time series of TC storm surge levels (Dullaart *et al.*, 2021). For all other types of storms, forcing data from the ECMWF Reanalysis v5 (ERA5) global climate reanalysis was used (Hersbach *et al.*, 2020). In the last step, tidal levels were sampled randomly and combined with surge to obtain ST levels, from this data the ST RPs were computed. The RPs were combined in a global dataset named COAST-RP (Dullaart *et al.*, 2021).

To model inundation in a dynamic way, time series of ST levels are required. For this, hydrographs that define the typical shape of an extreme ST level were used (Dullaart *et* *al.*, unpublished manuscript). Maximum water level data from the COAST-RP dataset was used to generate the hydrograph. Figure 7 displays an example of the 1 in 100-year ST hydrograph for a location closest to Bonaire.

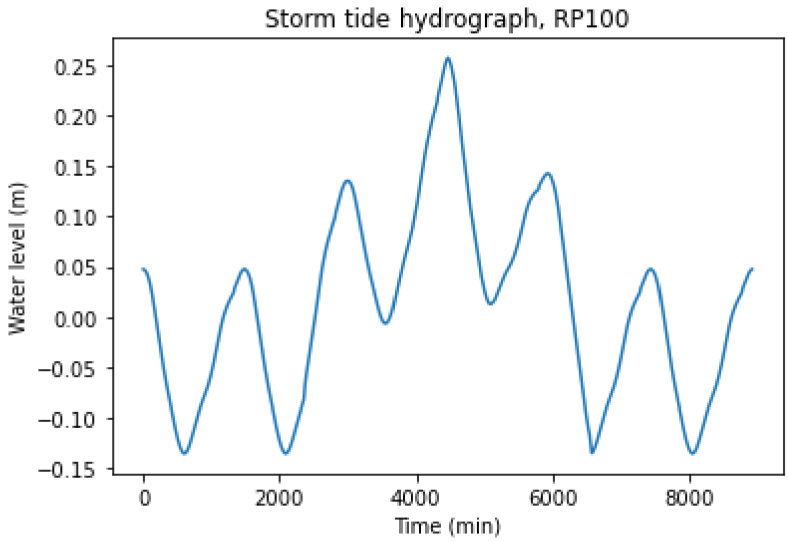

Figure 7 Example of a ST hydrograph of the 1 in 100-year RP of the location closest to Bonaire. The hydrograph shows the water level (m) over time (min) (Dullaart et al., unpublished manuscript).

The hydrographs for the locations closest to Bonaire were selected, resulting in 4 ST locations. All hydrographs have a temporal resolution of 10 minutes and a total length of 8940 minutes (Dullaart *et al.*, unpublished manuscript). For the dynamic inundation modelling WSU was added to the ST hydrograph, which will be further explained in the next section.

3.1.3 Wave set-up

Besides the ST, WSU was modelled in the dynamic inundation model as water level input. From the Copernicus Climate Change Service (C3S), significant wave height of wind waves and swell was downloaded. This parameter represents the combined height of the surface ocean waves generated by wind and swell and is part of the ERA5 global climate reanalysis (Hawker *et al.*, 2022). ERA5 data here provides hourly estimates of atmospheric, ocean-wave and land surface climate parameters; based on a reanalysis combining modelled data and observations from across the world. The horizontal resolution is 0.5° by 0.5° and a temporal resolution of 1 hour for the ocean-waves data which is available from 1979 to present (Hersbach *et al.*, 2018).

In this study, the extreme significant wave height was obtained by calculating the RPs from the annual maxima, similar to Muis et al, (2020). For each grid point, the annual maxima were selected for the period 1979-2021, creating a sample size of 42 maxima. To estimate the height of the WSU after the ocean wave breaking on the shore, the significant wave height was multiplied with the factor of 0.2 (Vousdoukas *et al.*, 2018). Subsequently, a Weibull distribution is fitted to the annual maxima of the WSU for every grid point, to estimate the wave height RP. For the coastal inundation modelling in SFINCS, only the 1 in 100-year RP is used.

After the maximum height of the WSU for Bonaire was obtained, the temporal component and the hydrological shape of a wave simulation was acquired. The time period between two consecutive wave peaks is estimated at 10 seconds (Hughes, 2016). Further, based on the study by Peachey (1986), the hydrological form of a wave is simplified to the shape of a sinusoidal with the formula:

$$wave\ height = vertical\ shift + amplitude * \sin\ ((2*\pi/period) * x - phase\ shift$$

Where:

vertical shift = 0 (m)
amplitude = 0.71 (m)
period = 10 (s)
x = time (s)
phase shift = 2.5 (m)

With this formula the WSU timeseries was generated. The vertical shift is set to 0, because the wave height is assumed to be 0 directly in between two waves (Hughes, 2016). The phase shift is set to 2.5 to generate a sinusoidal shape including the maximum wave height. Figure 8 shows the first 30 seconds of this timeseries, including 3 consecutive waves. The length of the series was set to the same extent as the ST hydrographs (8940 minutes = 536.400 seconds). Then, the ST hydrograph was resampled to a 1 second time step and interpolated linearly. Eventually, the WSU is added to the ST hydrograph.

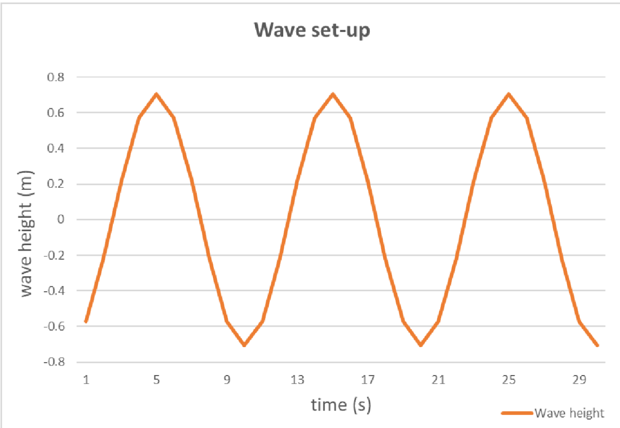

Figure 8 The first 30 seconds of the modelled time series of the WSU, showing three consecutive waves. The wave height (m) is shown over time (s)

3.1.4 Digital elevation model (DEM)

A DEM is the digital representation of the land surface elevation relative to a chosen reference point (Balasubramanian, 2017). In flood modelling, representative surface elevation data is of substantial importance to determine flood extent and inundation depth. The DEM used in this research is the so-called FABDEM (Hawker et al, 2022). This is the first global DEM with forests and buildings removed from the Copernicus GLO 30 DEM. A DEM excluding trees and buildings represents the actual ground surface, which is important for more accurate flood simulations (Hawker *et al.*, 2022). The FABDEM dataset is available at 1 arc second grid spacing, which is approximately 30 by 30 metres.

Furthermore, the FABDEM is referenced to the EGM2008 geoid model (Hawker *et al.*, 2022). This geoid model has a different vertical reference system as the ST hydrographs, namely WGS84 (Dullaart *et al.*, unpublished manuscript). Due to this dissimilarity, the water levels and the DEM contain a different vertical reference. Therefore, an adjustment in the vertical reference of the water level compared to the DEM was needed. The mean dynamic topography map by Andersen & Knudsen (2009), illustrates the vertical reference difference between the two geoid models. On Bonaire, the vertical reference of the WGS84 geoid model is 0.38m lower compared to the EGM2008 geoid model. Therefore, the hydrograph is corrected by adding 0.38m to the water level (Andersen & Knudsen, 2009).

3.2 Coastal inundation models

3.2.1 Static inundation models

Bathtub modelling is the most widely used GIS technique for inundation modelling (Schmid *et al.*, 2014; Vousdoukas *et al.*, 2016; Williams & Lück-Vogel, 2020). This is because it is relatively easy to implement and has a low computational demand. A bathtub simulation indicates which areas are flooded under a certain water level; in other words, observe what area is inundated when filling a bathtub to a certain water level. Besides a maximum water level, the only essential input requirement is a DEM. A higher spatial resolution of the DEM results in more accurate model outputs (Leon *et al.*, 2014; Williams & Lück-Vogel, 2020). In coastal flood modelling, bathtub inundation models often overestimate flood extent, especially when storm events are simulated. This is mainly due to the absence of a temporal component, as the maximum water levels are maintained for an infinite duration in the bathtub model. Also the lack of landscape characteristics and the exclusion of water flow equations causes an overestimation during storm events (Barnard *et al.*, 2019). Nevertheless, bathtub modelling is considered sufficient for simulating SLR, as this is a relatively constant water level, making the temporal component of less relevance (Schmid *et al.*, 2014; Vousdoukas *et al.*, 2016). Permanently inundated areas due to SLR give an indication of moving coastlines. Therefore, the bathtub model is used to simulate future coastlines on Bonaire under different climate scenarios.

The bathtub methodology in this research follows a similar approach as the studies by Yunus *et al*., (2016) and Poulter & Halpin (2008). In these studies, a grid cell floods when the elevation is below the water level and when the grid cell is connected to an adjacent grid cell that was flooded or that is open water. Using the QGIS environment, the following procedure was taken to determine permanent inundation on Bonaire. First, a new water level raster of the same size and resolution as the DEM was created, where every cell had the same value of the SLR scenario. Then, the DEM was subtracted from this water level raster, creating a layer with the water depth at every location on Bonaire. All negative values, representing the non-inundated areas, were reclassified to 0 with the function '*Reclassify by table*'. With the '*r.clump*' function, all areas below the water level, but not connected to the sea, were selected and then masked from the final inundation map created with the *'r.mask.rast'* function. This procedure was applied for all simulations, creating an inundation file for every scenario. The resulting map indicates the projected flood depth and extent of the modelled climate scenario.

3.2.2 Dynamic inundation modelling

To incorporate the dynamic component of ST and waves into a simulation, the reduced-physics model SFINCS was used (Leijnse *et al.*, 2021). The SFINCS model is developed as a tool to efficiently simulate compound flooding for coastlines up to thousands of kilometres long. The model is considered computational efficient, because it only includes the necessary processes of compound flooding with a simple and fast numerical solver. For example, SFINCS simplifies the equations of momentum and mass conservation, which are important to calculate flow dynamically. Other processes that currently can be incorporated in the model are: spatially varying friction, infiltration, precipitation, wind-driven shear and wave-driven processes. This makes SFINCS the first reduced-physics model relevant for simulating coastal compound flooding with the inclusion of fluvial, pluvial, tidal, wind and wave processes (Leijnse *et al.*, 2021). SFINCS is a dynamic inundation model, meaning that it is possible to incorporate the time dimension into the simulation. Integrating the time dimension is important to accurately model temporal varying forcing inputs, such as ST and waves (Barnard *et al.*, 2019). However, like every model, also SFINCS has its limitations. Currently, there are three important limitations of the SFINCS model that are relevant for this study (Leijnse, 2021). First, it is unknown how the model compares in accuracy and efficiency to unstructured full-physics models (e.g. Delft3D-FM). These models are deemed to have a more optimal grid resolution and therefore a high accuracy. Second, SFINCS does not include for Coriolis effect, viscosity and the effects of atmospheric pressure gradient. This is believed to have a low impact on inundation results for inland modelling, however, this has not been assessed yet. Last, initial water levels of estuary landward were underestimated in prior case studies by Leijnse, (2021). On Bonaire this is relevant for the modelling results around the area of Lac Bay.

With the limitations in mind, the next step is to explain how the model was set up. The SFINCS model requires several input files to subsequently produce inundation maps for the climate change scenario's on Bonaire. The first step before running a SFINCS model is building the environment in which the model can run its simulations. This environment is created with the python package Hydro Model Tools (HydroMT), in which it is possible to build and analyse the SFINCS model (Eilander *et al.*, 2022). Within the HydroMT tool, the 'hydromt build sfincs' command built the SFINCS model with a specification of the *bounding box*, *configuration file* and the *data catalogue file*. The bounding box defines the area of the model, specified with coordinates. In the *configuration file (.ini)* the required parameters are stored, from which the model can access and read the needed input files and model settings (e.g. topography data, mask parameters, start time, stop time, time step and water level forcing). The configuration file applied in this study can be found in Appendix A. All model parameters that are not defined in the *configuration file* are set to the default settings of the model. Lastly, the *data catalogue file (.yml)* calls the needed spatial data, specifying their coordinate system, data type and folder path. It also provides the references to the input files in the meta data and can be read in Appendix B. The most important topographical input files used by the model besides the DEM include: a bathymetry file (GEBCO Compilation

Group., 2021), a land use file representing the roughness of the landscape (Buchhorn *et al.*, 2020) and a global curve number file used for soil infiltration rates (Jaafar *et al.*, 2019). Lastly, for the hydrography on Bonaire, the MERIT Hydro dataset was used. This global dataset incorporates flow direction, flow accumulation and river channel width (Yamazaki *et al.*, 2019)

After the HydroMT environment was built, the SFINCS model was run with the following important input settings described in the *sfincs input file (.inp)* (Appendix C). The horizontal resolution of the model was set on 20m to keep it computational efficient for the size of the research area. The time span of the simulation was 7 days, with output calculations after every 600 seconds for the output files. Additionally, the advection term is set to 0, meaning that the movement of water through the atmosphere is neglected. Normally, the use of the advection is recommended when modelling waves, however, it seemed to have no effect on the model simulation. This is likely because of the low resolution of the simulations. Furthermore, for every simulation including all three water level forcings, a restart simulation was modelled beforehand. This simulation creates a *restart file* containing output with only SLR as forcing input. The restart simulation was modelled over the same time period, but with the constant water level of the predicted SLR. The final water levels of the restart simulation are then set as the starting point for the simulation including SLR, ST and WSU. Therefore, the model is adjusted to the constant water level of SLR before the modelled storm, creating a more realistic future storm simulation. (Leijnse, 2022).

Lastly, after each SFINCS model simulation a *sfincs_map.nc* was created as an output file. This file contains the water level for every cell in the model for every time step. From this output file, a raster containing the maximum water level was created using the *hydromt_sfincs* package (Eilander *et al.*, 2022). The maximum water level is the main output used for the inundation scenario analysis which described the final results.

3.3 DEM validation

The DEM is an important model input in estimating the potential future inundation on Bonaire. The FABDEM used in the model simulations is validated using two different approaches: field measurements and an alternative DEM. The first approach is based on field elevation measurements. Elevation measurements were taken at the seawall of Kralendijk during a field trip on Bonaire. As the seawall is a vertical structure directly on the coastline, it was possible to measure the elevation above sea level with a measuring tape (Figure 9). Eleven field measurements were taken at different locations along the coast. Unfortunately, not all locations were suitable for measurements due to private property or non-vertical slope angles on the coast. The height of the seawall was measured from the water level to the ground surface, whereafter all measurements were corrected for the tides of the measurement day, May 10th, 2022 (Tide schedule in Bonaire, 2022). To compare the field measurements with the FABDEM elevation levels, the FABDEM elevation was reduced by 38 cm to correct for the difference in vertical reference level (Andersen & Knudsen, 2009). Besides field measurements, 5 more elevation observations were retrieved via Geomaat Caribe B.V. (2022), a Bonairian surveyor company.

The 11 field observations and 5 elevation observations retrieved by Geomaat showed a substantial deviation from the FABDEM used in the simulation; all 16 observation points are lower than the FABDEM elevation height (Appendix D). On average, the FABDEM is 1.2 m higher compared to the field observations. To adjust for this large deviation, a recalculated DEM was created by applying a correction factor of -1.2 m. This corrected DEM was then used to simulate a low-end (SSP1-2.6, 2050) and high end (SSP5-8.5, 2150) inundation model. Both simulations were analysed in comparison to the original FABDEM simulation. The assumption of a general 1.2 m overestimation by the FABDEM is based on a small set of observations, therefore no hard conclusion can be drawn from the analysis. However, it gives an indication of the uncertainty of the FABDEM in estimating the flood extent.

The second DEM validation approach regards validating the FABDEM with a different DEM, named CoastalDEM (Kulp & Strauss, 2018). The CoastalDEM has the same resolution as the FABDEM, making the quality of the DEM comparable. Two additional SFINCS simulations were made with the CoastalDEM as topographic input data, for the high-end SSP5-8.5 scenario in 2150 and for the low-end SSP1-2.6 scenario in 2050. A high and low-end scenario were chosen to validate the DEM on two different extremes. The results of the CoastalDEM simulation are compared to the FABDEM results of the same climate.

Figure 9 Photo of one of the elevation measurements in Kralendijk, illustrating the difference between the measured and the FABDEM elevation

3.4 Coral reef simulation

The ocean near the coast of Bonaire contains coral reefs, which are a natural coastal protection against waves and storm surges (Ferrario *et al.*, 2014). A case study from the Seychelles analysed the effects of coral reef degradation on the total wave energy that reaches the shore (Sheppard *et al.*, 2005). Their model indicated that 20 years after the degradation, the wave energy that reaches the shore increased on average with 80%. Therefore, to simulate flood hazards on Bonaire with degraded coral reefs, the WSU was assumed to increase with this percentage as well. For the WSU calculations in the model, the WSU factor of 0.2 (Vousdoukas *et al.* 2018), was multiplied with 1.8, resulting in a WSU factor of 0.36. With this new factor the wave height was recalculated and a scenario with coral reef degradation was simulated. This is done for the middle of the road scenario SSP2-4.5 in 2050. This scenario is chosen, because SLR is still small compared to 2150. Therefore, the degraded coral reefs had a relatively larger effect on the modelled floods in this scenario.

3.5 Inundation scenario analysis

Before elaborating on the results of the two coastal inundation models, a summarising list of all modelled scenarios is given. Most scenarios are dependent on the water level forcings; multiple SLR scenarios were acquired, while only the 1 in 100-year RP of ST and WSU was used. The complete list of modelled scenarios is as follows:

- Bathtub model:
  - All SSP SLR scenarios from Table 3
- SFINCS model: All scenarios include the 1 in 100-year RP for ST and WSU
  - All SSP SLR scenarios in Table 3
  - A reference scenario of the current climate. Excluding SLR.
  - Simulation with recalculated DEM for validation: scenario SSP1-2.6 in 2050 and SSP5-8.5 in 2150.
  - Simulation with CoastalDEM for validation: scenario SSP1-2.6 in 2050 and SSP5-8.5 in 2150.
  - Coral degradation simulation: scenario SSP2-4.5 in 2050.

After all scenarios were simulated with the bathtub or SFINCS model, the results were analysed. Flood maps were created using QGIS, making it possible to visually compare the different scenarios. Furthermore, both QGIS and Microsoft Excel were used to calculate and visualize variations in inundation characteristics, such as flood extent and depth. Hereafter, the most important results will be discussed and visualized. With the results from the bathtub model, the future coastlines of Bonaire will be compared within the different climate scenarios and time periods. The results of the SFINCS model will be analysed similarly, however also the flood prone areas under storm conditions will be determined and the changes in flood extent will be analysed. Lastly, the results of the validation and coral degradation simulations will be compared to the results of the regular SFINCS simulations of the same climate scenario.

4 Results

After all simulations were run and the analysis was made, the most important results are presented here. First, the results of the bathtub model are exhibited. Then, the main findings of the dynamic SFINCS model and the coral degradation simulation are shown. Lastly, the final results of the DEM validation is presented.

4.1 Future coastlines

In this section, the results of bathtub modelling will be provided. As SLR is the only water level forcing established in the bathtub model, the following results illustrate the possible future coastlines of Bonaire under the multiple climate scenarios. Because the differences in projected SLR per scenario are largest in the far future, the 2150 and 2300 results will be illustrated here. The individual inundation maps of all scenarios can be revised in Appendix E.

4.1.1 Coastline of 2150

Figure 10 illustrates the projected coastlines in 2150 for the scenarios: SSP1-2.6, SSP5-8.5 and SSP5-8.5 LC. These scenarios were chosen, because it shows the widest range of possible future coastlines. The expected SLR in 2150 ranges from 0.78 to 2.19 meters, SSP1-2.6 to SSP5-8.5-LC. Here, the coastline extent of the three scenarios will be discussed.

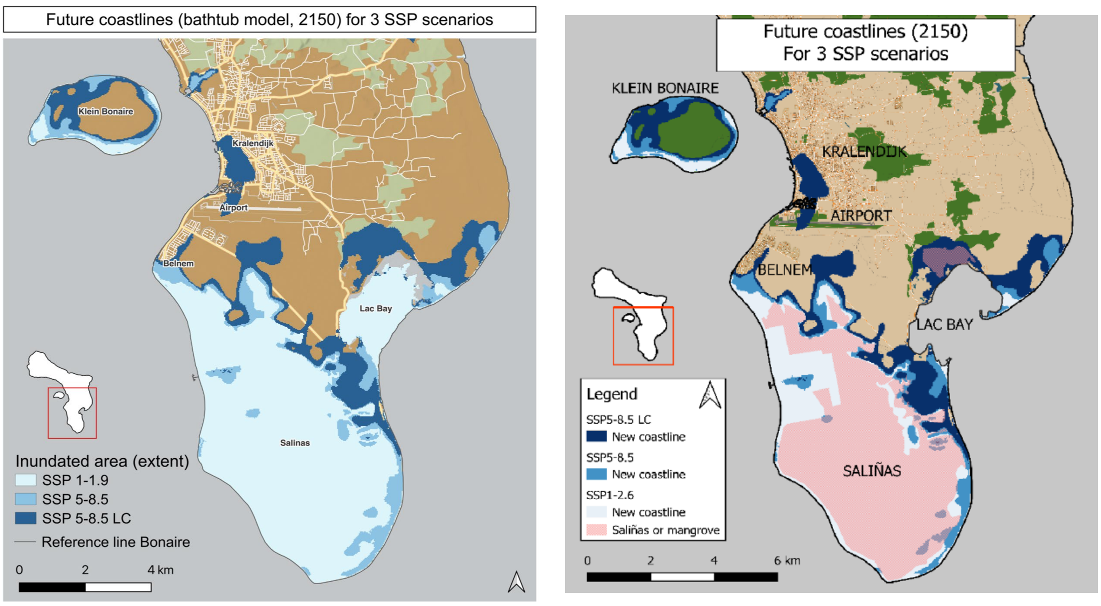

Figure 10 Inundation map illustrating the future coastlines of Bonaire in 2150 under SSP scenarios: SSP1-1.9, SSP5-8.5 and SSP5-8.5 LC

First, in the low-end SSP1-1.9 scenario, the effect of SLR is limited to the most southern part of the island and Klein Bonaire. The coastline will move northwards up to Belnem and all of the saliñas will be taken by the ocean. Furthermore, small southern and eastern parts of Klein Bonaire and Lac Bay will be permanently inundated.

Then, looking at the SSP5-8.5 projection, it can be seen that the difference in flood extent is relatively small. The coastline slightly extends north- and eastwards from the saliñas again, also permanently flooding the southern part of Belnem as well as Sorobon on the east coast . Other urban areas, such as Kralendijk and the airport will not be permanently flooded by SLR under the high-end SSP5-8.5 scenario.

Lastly, the most extreme scenario is SSP5-8.5-LC. The flood extent of this scenario is substantially the largest, including large inundated areas north of the saliñas, but also north and east of Lac Bay. Also, large parts of Klein Bonaire are permanently flooded, shrinking the island to half its current size. However, the most critical difference with the other scenarios is the large inundated area around Kralendijk and at the airport. In this scenario, SLR exceeds the lowest point of the seawall directly on the coast of Kralendijk. This causes the lower parts of Kralendijk, directly behind the seawall, to flood. Figure 11a illustrates this bowl-shaped area behind the higher elevated coastline, while Figure 11b shows the downward slope from the seawall at the ocean land inward. In the bathtub model, this relatively lower part of Kralendijk only floods when the water level exceeds the lowest point of the seawall. This is because only cells connected to the ocean can flood in the model (Yunus et al, 2016; Poulter & Halpin, 2008).

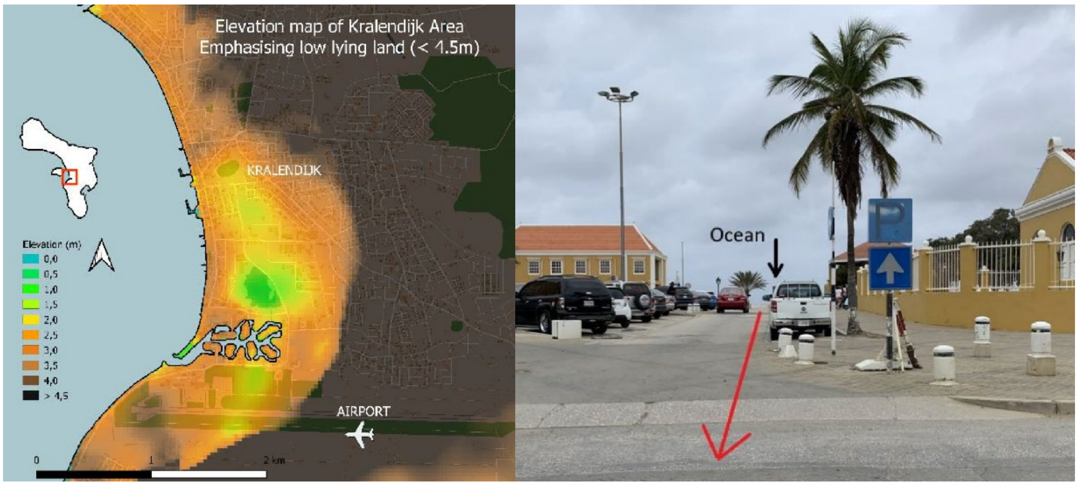

Figure 11 Left) Elevation map of Kralendijk, illustrating the low-lying bowl-shaped area. Right) Photo of Kralendijk indicating the downward slope from the ocean land inward

4.1.2 Coastline of 2300

As climate change is expected to have long standing effects on SLR, there are large differences projected in SLR between the climate scenarios in the far future (IPCC, 2021). This large difference can be seen by the estimated SLR in 2300. For scenarios SSP1-2.6 LC the projected SLR is 1.05m and for scenario SSP5-8.5 LC 4.05m.

As a consequence of the large difference, the modelled coastlines in 2300 are dissimilar as well (Figure 12). The low-end scenario shows a new coastline north of the saliñas at Belnem, whereas also small parts at Lac Bay and Klein Bonaire will also be permanently inundated. Contrary to the low-end scenario, SSP5-8.5 LC indicates a future coastline far inland and overlying large populated areas. In Kralendijk, the coastline will move almost 2 kilometres landward, while also most of Belnem will be permanently inundated. Similar to Belnem, almost the whole of Klein Bonaire will be permanently flooded.

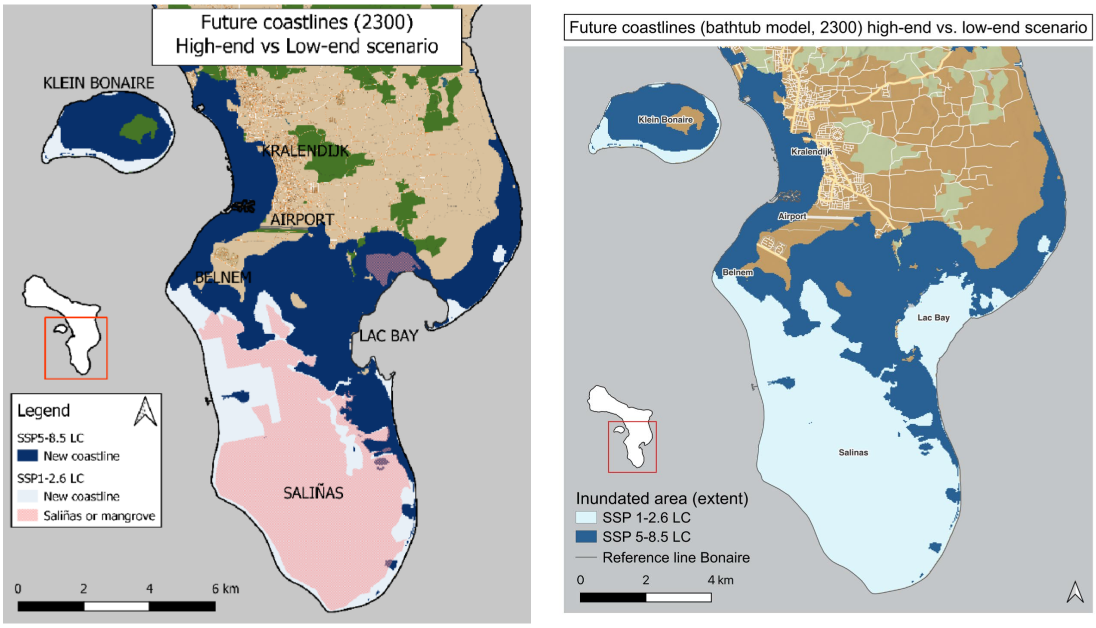

Figure 12 Inundation map illustrating the future coastline of Bonaire in 2300 under SSP scenarios SSP1-2.6 LC and SSP5-8.5 LC

4.2 Future storm impact

Here, the results of the dynamic inundation modelling are presented. Besides the water level forcing of SLR, also the 1 in 100-year ST and WSU is included in the SFINCS model. Therefore, the following results give a representation of the future storm inundation impacts. As there are 15 unique combinations in climate and temporal scale, not all inundation maps will be exhibited in this section. The results of the middle of the road scenario SSP2-4.5 are shown for 2050 and 2100. Whereafter all climate scenarios for the year 2150 are displayed as well. All SFINCS inundation maps can be found in Appendix F.

4.2.1 Current climate storm impact

Before describing the impact of inundation hazards for possible future climate scenarios, it is important to look at the current inundation risk on Bonaire. Figure 13 shows the inundation map of the 1 in 100-year ST and WSU under the current climate. The inundation depth extends up to 1 meter deep in the low-lying areas. In terms of flood extent, inundation occurs mostly in the saliñas, the mangroves at Lac Bay and the south of Klein Bonaire; locations that are already known to be permanently inundated. Yet, a small area south of Belnem is flooded in this model simulation, with inundation up to a few centimetres. There is no inundation simulated in more densely built-up areas, such as Kralendijk.

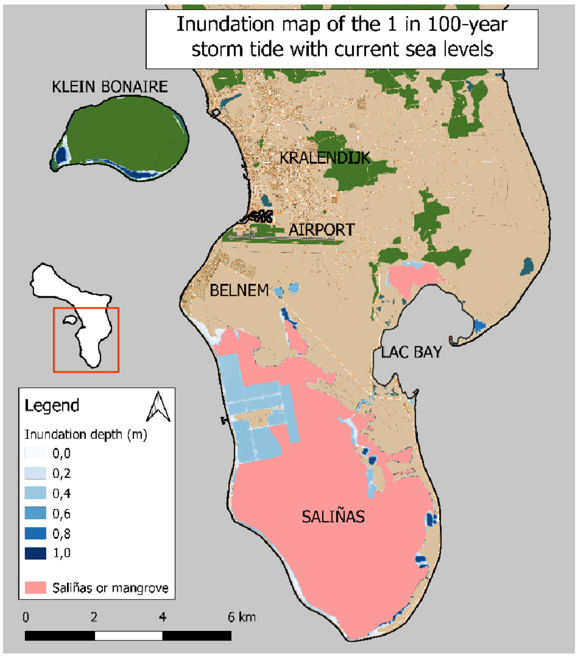

Figure 13 Inundation map of the 1 in 100-year RP storm under current sea levels

Following, the results including the future climate projections are shown here. To indicate the difference between the SSP scenarios and the temporal scale, the total inundated surface area is calculated (Figure 14). The calculations exclude the surface area of the saliña and the mangroves of Lac Bay, as this is already permanently inundated. The climate scenarios are divided into the three main temporal classes: 2050, 2100 and 2150. The differences between those classes will be discussed next.

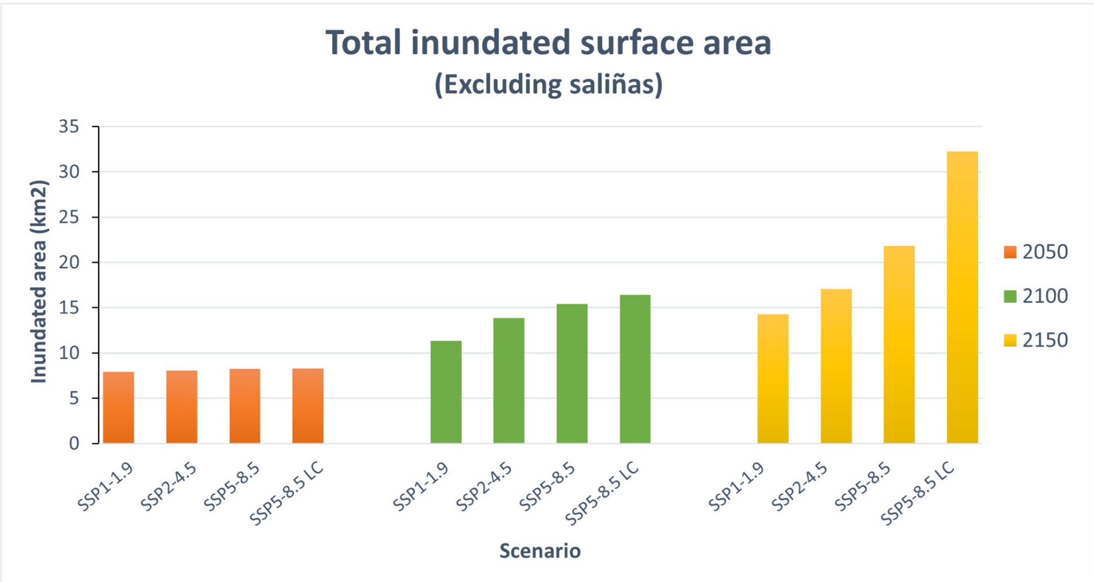

Figure 14 Histogram showing the SFINCS simulations total inundated surface area of all scenarios is 2050, 2100 and 2150. The saliñas and mangroves are excluded from the total inundated surface area, because this is already permanently inundated

4.2.2 Storm impacts 2050, 2100 and 2150

To begin with 2050, Figure 14 depicts the small difference in flood extent between all scenarios in 2050. The total inundated surface area is between 8.0 and 8.3 km2. The reason for this small distinction between the scenarios is that the expected SLR is very similar for all SSPs. Because of this small difference, only the inundation map of middle of the road scenario, SSP2-4.5, is described (Figure 15). This inundation map shows similar results as the simulation representing a storm under current climate conditions. (Figure 13). A slight increase in inundation depth, as well as a slight extent northwards towards Belnem, can be noticed.

Secondly, a broader distinction in flood extent is observable at the end of this century (Figure 14). The total inundated surface area ranges from 12.2 to 16.4 km2. Even though the differences in flooded area between the SSP scenarios becomes larger in 2100, the inundated locations are still similar in all scenarios. Inundation occurs mainly at the saliñas, Lac Bay, Klein Bonaire and south of Belnem. Therefore, only the inundation map of the middle-road scenario SSP2-4.5 will be discussed here (Figure 16). In 2100, inundation is simulated more northwards from the saliñas, into the built-up area of Belnem. Nevertheless, no inundation is expected in economically important regions such as Kralendijk or the airport.

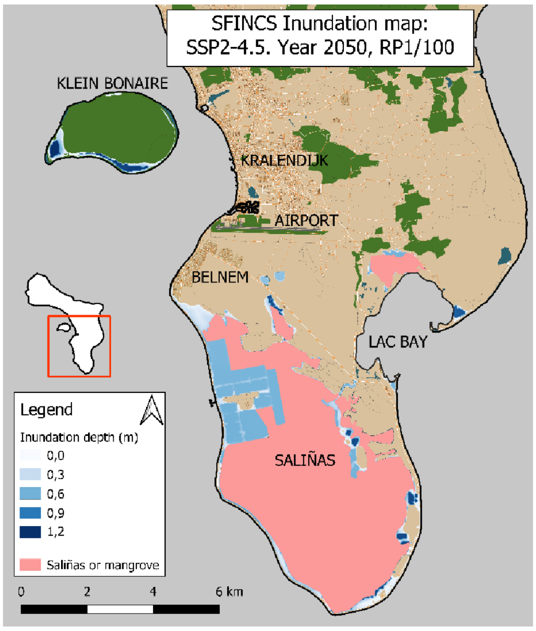

Figure 15 Inundation map of scenario SSP2-4.5 in 2050

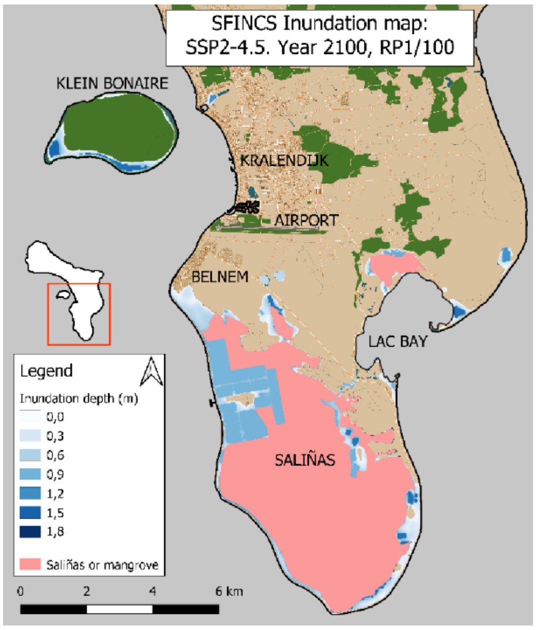

Figure 16 Inundation map of scenario SSP2-4.5 in 2100

The last SFINCS simulations discussed here are the ones for the year 2150. Due to the largest differences in projected SLR, the simulations show the greatest variation. Inundated surface area more than doubles comparing the low-end and high-end LC scenario (Figure 14). The total flood extent ranges from 15 to 32 km2 in 2150. To zoom in on the local differences between the scenarios, Figure 17 illustrates the inundation maps focussed on the Kralendijk area. The most important distinction is between scenario SSP2-4.5 and SSP5-8.5. This is because in the latter simulation, also parts of

Kralendijk become inundated. Furthermore, larger areas around Lac Bay and on Klein Bonaire are predicted to flood. In the most extreme SSP5-8.5 LC scenario, substantially greater areas of Kralendijk are expected to flood. The same applies to the airport, which in 2150 is only inundated in this most extreme scenario. Lastly, in comparison to the first three scenarios, also significantly large parts of Belnem, Lac Bay and Klein Bonaire are predicted to flood in the SSP5-8.5 LC scenario. This, in combination with the deep inundation depth, make this a potentially destructive scenario.

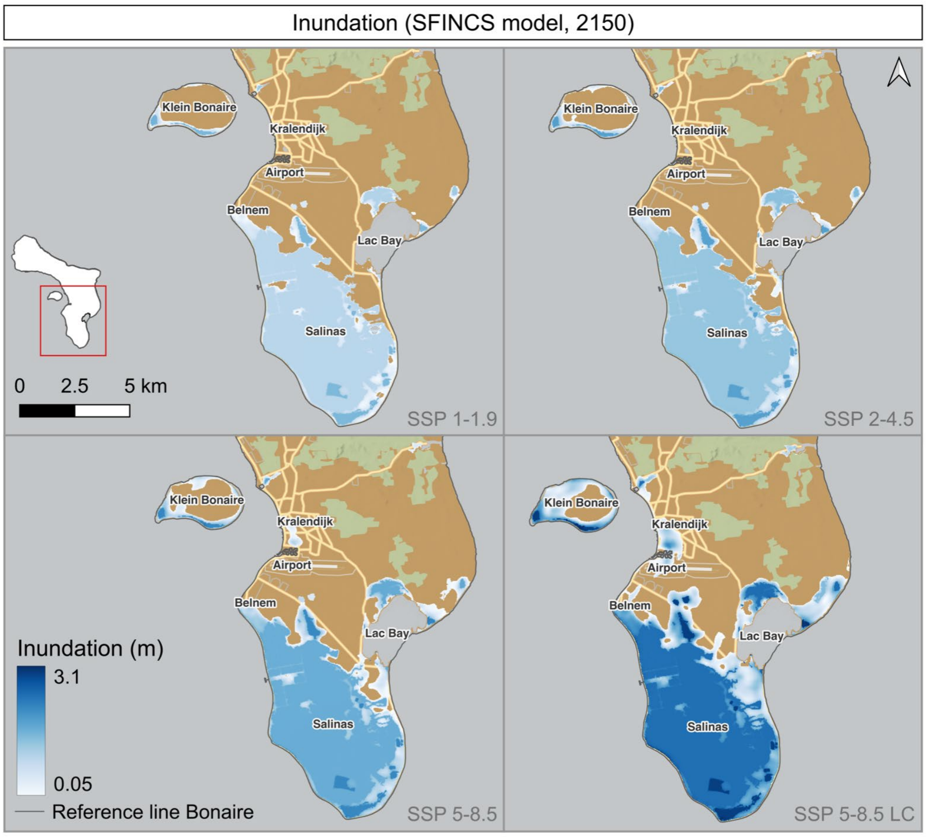

Figure 17 Inundation maps of all modelled SSP scenarios in 2150: SSP1-1.9, SSP2-4.5, SSP5-8.5 and SSP5-8.5 LC, including the 1 in 100-year RP

4.3 Coral degradation comparison

Here, the impacts of coral degradation on coastal flooding is illustrated. Figure 18b shows the projected inundation difference between a healthy and completely degraded coral reef for the SSP2-4.5 scenario in 2050, taking the 1-in-100 year storm event into account using the SFINCS model. As reef degradation increases WSU with 80%, also flood extent increases. The total inundated surface area, excluding the saliñas, increases with 41%, from 8.0 to 11.3 km2 (Figure 18a). Inundation depth increases with an average of approximately 0.24m, with a larger increase directly on the coastline.

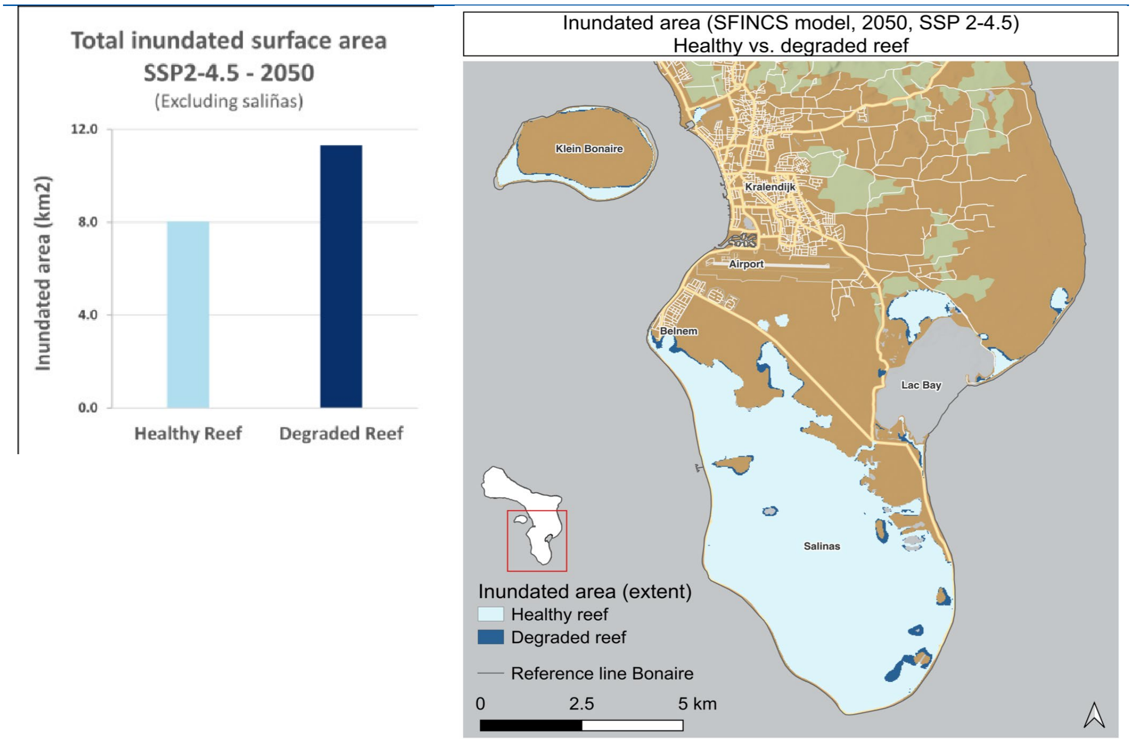

Figure 18 Inundation map illustrating the difference in flood extent between a healthy and degraded reef for scenario SSP2-4.5in 2050, including the 1 in 100-year RP

4.4 DEM validation results

The FABDEM is validated following two approaches. First, based on observed elevation measurements and thereafter with the CoastalDEM. The results of both validation techniques are shown next.

4.4.1 FABDEM correction

The comparison between the corrected DEM and the FABDEM, for scenario SSP5-8.5 in 2150 using the SFINCS model, is portrayed in Figure 19. As a consequence of the DEM correction factor of -1.2m, flood extent increased with 53%, with the saliñas excluded (Figure 19a). This large increase can be seen in all locations on the south of Bonaire. However, especially the flood extent around Kralendijk and the airport became significantly larger. The simulation of the low-end scenario SSP1-2.6 in 2050 (Appendix G) modelled an even larger flood extent increase of 94%. The reason for this even larger increase is that the DEM correction is relatively large compared to the difference in water level between the high and low-end scenarios.

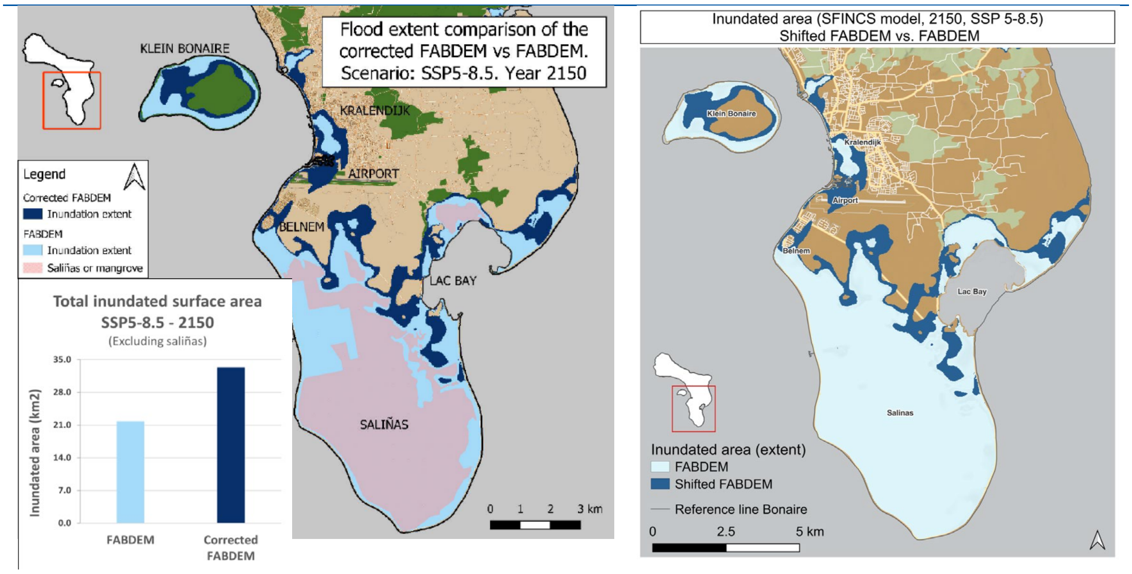

Figure 19 a) Histogram showing the difference in total inundated surface area between the FABDEM and the corrected FABDEM. b)Inundation map illustrating the difference in flood extent between the FABDEM and the corrected FABDEM for scenario SSP5-8.5in 2150, including the 1 in 100-year RP

4.4.2 CoastalDEM and FABDEM

Figure 20b shows the difference in flood extent between the CoastalDEM (dark blue) and the FABDEM (red) for the high-end SSP5-8.5 scenario in 2150. The light blue colour indicates inundation in both DEMs and demonstrates that both are quite similar in flooded area. In numbers, the total inundated surface area is 4.8% higher for the FABDEM (Figure Xa). Especially around Lac Bay and Belnem, more inundation is projected by the FABDEM. On the other hand, the CoastalDEM projects more inundation directly on the coastlines. From north of Kralendijk down to Belnem, as well as on the east coast, a thin stroke of inundation is simulated directly on the coastline. Comparable results were found for the same analysis with a low-end SSP1-2.6 scenario in 2050 (Appendix G). The FABDEM projection simulated 15.9% more inundation compared to the CoastalDEM.

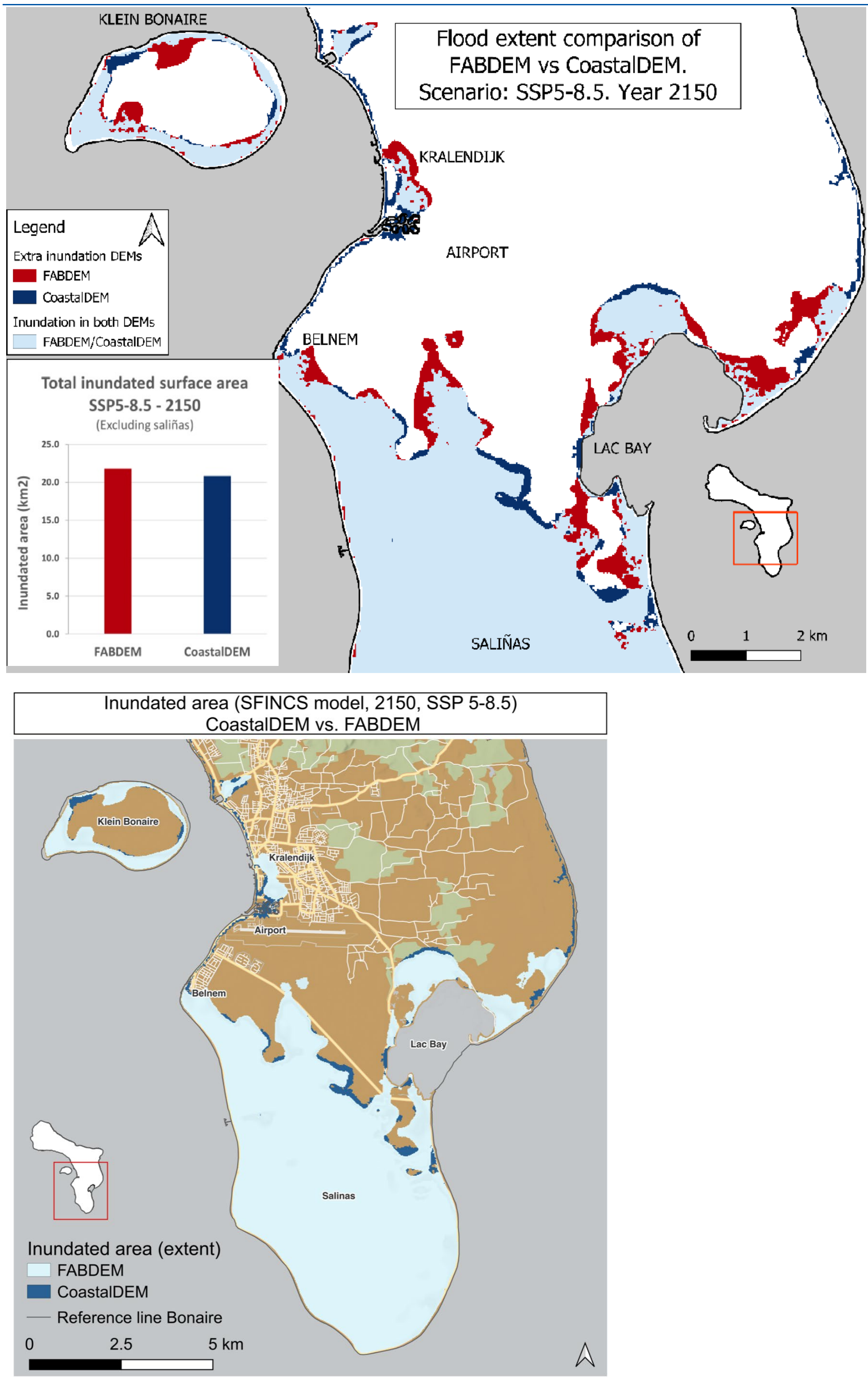

Figure 20 Inundation map illustrating the difference in flood extent between the FABDEM and the CoastalDEM for scenario SSP5-8.5 in 2150, including the 1 in 100-year RP

5 Discussion and recommendations

Although the results of the coastal inundation models have indicated that substantial parts of the south of Bonaire will endure increased flood risk in the future, coastal flooding on Bonaire deserves further additional research. In the discussion that follows, the first implications of the results will be explained, where after multiple issues concerning the input data and the models itself will be debated. First, the consequences of the new coastlines and storm impacts will be considered. Then, the quality of the FABDEM will be discussed, based on the DEM validation results. Subsequently, the drawbacks of the water level forcing input data will be evaluated. And lastly, the degraded coral reef simulation will be debated.

5.1 Future implications for Bonaire

Now the results from the two inundation models are described, several implications for the future of Bonaire fold out. To begin with, it is clear from both models that SLR and the effect of storms will firstly impact the low-lying nature reserves of the saliñas, Lac Bay and Klein Bonaire. This can already negatively affect the island through the impact on the valuable ecosystem services they provide (Van der Lely *et al.*, 2013; Schep *et al.*, 2013). From 2050, the coastline will move up northwards towards the first built-up areas of Belnem. Then, similar consequences are projected for 2100, however, with pronounced differences between the climate scenarios. Finally, from 2150 the implications for Bonaire start to become critical under high-end climate scenarios. From this point in time, storms are expected to largely affect Kralendijk when climate change will follow a SSP5-8.5 scenario. On the other hand, when climate change is contained within the scenario of SSP2-2.6, both the future coastline and the impact of storms will be limited to the low-lying nature reserves. This difference indicates the importance of limiting climate change for an adaptable future on Bonaire.

What is more, the results of the bathtub and SFINCS models are quite similar. The projected inundation of the SFINCS simulations are only slightly enlarged compared to the same scenario in the bathtub model. As the SFINCS model is forced with ST, waves and SLR and the bathtub model only with SLR. This small difference between the models indicates that SLR is the most important water level forcing of the three. The degradation of coral reefs that could lead to a 24 cm increase in wave height during a 1-in-100 year storm does not change this conclusion. Therefore, future SLR is considered more crucial compared to the future impacts of storms on Bonaire.

5.2 FABDEM validation

As stated by Williams & Lück-Vogel (2020), the DEM quality is of great importance in flood modelling. Evidently, the DEM validation results confirmed this statement, as flood extent increased enormously due to the DEM correction (53% and 94%). However, with only 16 field observations, the recalculation of the corrected DEM are based on extremely simplified assumptions. Therefore, the results of the inundation model that include the corrected DEM, cannot be seen as valid projections for the future. Yet, from the large increase in flood extent of 53% and 94%, it can be inferred that a higher quality DEM is needed to model more accurate inundation simulations.

One DEM that was considered potentially more accurate, was the CoastalDEM. This DEM has a vertical bias on the coastal areas of the United States of less than 0.01m, compared to 3.67m in other global DEM datasets (Kulp & Strauss, 2018). This is a great improvement of global DEMs; however, it should be noted that the CoastalDEM is only trained on US and Australian lidar data. Therefore, the CoastalDEM might not be trained sufficiently for different locations in the world, like Bonaire. The results comparing the inundation of the FABDEM and the CoastalDEM didn't show large deviations. Besides, it is difficult to analyse which DEM performed better in the end. For this, more elevation measurements are needed to validate both DEMs on the actual elevation heights.

Until an accurate and high resolution global DEM is available, it is recommended to use multiple DEMs to construct an inundation uncertainty range that can be applied in flood risk management on Bonaire (McClean *et al.*, 2020). For the whole European Netherlands, a publicly available LiDAR DEM, on a 0.5m horizontal resolution, is accessible (PDOK, 2022). It is advisable to create a similar dataset for the Dutch Caribbean Islands to improve coastal inundation models. Currently, Wageningen University is working on such an improved DEM on a 1m resolution, which is expected to become available in 2022 (DCBD, 2022). Therefore, it is recommended to run the models in this study again when this data is accessible.

5.3 Water level forcing input data

First of all, multiple SLR projections from the IPCC (2021) were used to determine future coastal inundation. These projections are made by Global Climate Models, creating a range of projections forced by the selected SSP scenario. This leads to an uncertainty in the SLR projection that is therefore also used in this research. The level of uncertainty increases with time (IPCC, 2021). Therefore, the modelled inundation for 2150 and 2300 contains more uncertainty, compared to 2050 and 2100. In addition, the two LC SSP scenarios contain an even higher deviation due to specific ice sheet melting processes included in the IPCC (2021) models. As SLR is the most important water level forcing in this study, it is important to acknowledge these uncertainties when the results of this study are used in other flood risk related research (e.g. De Boer, 2022; Baertz, 2022; Buijs, 2022).

Thirdly, only one RP of the ST has been simulated. This is because of the relatively small difference between the 1-in-100 and the 1-in-1000 year storm tide on Bonaire (approximately 0.2m) (Dullaart *et al.*, 2021). Compared to the SLR forcing of 2.19m predicted for the most extreme SSP scenario, this difference is relatively small. Furthermore, in this study we assume that the 1 in 100-year RP remains the same towards the future. A fairly new study by Bloemendaal et al, (2022) generated a similar dataset of synthetic TCs as used in this study (STORM). However, this STORM dataset is forced with SSP5-8.5 climate conditions for the period 2015-2050. With this new STORM dataset, the RPs of extreme STs can be remodelled using the same approach as Dullaart et al, (2021), creating a new COAST-RP dataset for climate scenario SSP5-8.5. Consequently, more accurate future coastal inundation simulations can be made, with a similar approach as this research.

Furthermore, the water level forcing of waves includes some limitations. This is mainly due to the simplified approach that is used in this study for WSU formation by Peachey (1986). Here, a sinusoid is used as a simplification of the hydrological shape of a wave. However, the modelling of WSU is very complex, especially on shore (Johnson, 2006). Modelling waves in a more realistic way was unfortunately out of the scope of this research. However, in further research the complexity of WSU could be taken into account by using a numerical wave model approach as reviewed by Thomas & Dwarakish (2015).

Lastly, the scope of this study was focussed on modelling coastal flooding on Bonaire. For this, water levels of SLR, storm tide and WSU were used as input. However, other forcings can also contribute to the impact of the TCs, such as precipitation (Wahl *et al.*, 2015). This combination of water level inputs can be modelled with SFINCS and has been modelled before (Leijnse, 2018; Leijnse, 2021). Recently, on 29 June 2022, tropical storm Bonnie was expected to generate 100-150mm of rain on Bonaire (De Laat, 2022). To study the impact of compound flooding on Bonaire, it would be interesting to incorporate RPs of precipitation (e.g. Mélice & Reason, 2007) into this study.

5.4 Coral reef degradation

The increase of WSU simulated by the degraded coral reef resulted in an increase in flood extent of 41% in 2050. Accordingly, the degradation of coral reefs leads to an increased flood risk on Bonaire. Yet, it should be stressed that the model, simulating degraded coral reef, is an exaggerated simplification of reality. In this simulation, the degradation of the reef increases the height of the WSU based on the study by Sheppard *et al.* (2005). In that research, the effect of coral degradation on wave energy has been simulated on 15 different coral reefs. Wave energy increased in all simulations, however, the total increasement varies from about 50% to 250%. This large difference is caused by the various reef and ocean characteristics that affect WSU, e.g., slope angle, reef height, width and length, roughness, but also water level above the reef and therefore SLR (Sheppard *et al.*, 2005; Lugo-Fernández & Roberts, 2011; Ferrario *et al.*, 2014).

Thus, to obtain a more accurate estimation of the change in WSU caused by coral degradation on Bonaire, reef characteristics should be incorporated. Mücher *et al.*, (2017) completed a coral reef classification of Bonaire, based on hyperspectral imagery. The study provides a qualification of the reef types on Bonaire, making it possible to value the roughness of the reef. Furthermore, also a bathymetric model with a 1m spatial resolution is provided, making it possible to classify factors such as slope angle and water level. With these characteristics of the Bonairian reef a better valuation of the WSU can be made, based on the simulation by Sheppard *et al.*, (2005).

In addition, in this simulation, coral reefs are estimated to be completely degraded by 2050 with a middle of the road SSP scenario (SSP2.45). Yet, Gattusso *et al.*, (2014) estimated global coral degradation of 50% in 2100 under a similar climate scenario. Nevertheless, the results here still show the impact of the coral degradation on flood risk. The modelled climate scenario is of less relevance when the same scenarios are compared, because only the effect of the coral degradation will be visible.

6 Conclusion

The goal of this research was to assess the impacts of climate change on coastal inundation on Bonaire. Based on future SLR scenarios, a bathtub coastal inundation model projected the future coastlines of Bonaire up to the year 2300. Furthermore, a second coastal inundation model called SFINCS, simulated flood events by dynamically incorporating the water level forcing of SLR, storm tide ST and WSU. Lastly, a model assuming a completely degraded coral reef was simulated to assess the impacts of coral reef degradation on coastal inundation. By doing so, the implications of SLR, storm events and reef degradation were evaluated for different climate scenarios.

Based on the results of both the bathtub and the SFINCS model we can conclude that the impact of climate change on coastal inundation becomes critical for urban areas in the year 2150. From this time period, large parts of the capital Kralendijk are expected to be affected by storms under high-end climate scenario SSP5-8.5. By way of contrast, flood extent remains substantially smaller and is mostly limited to low-lying nature reserves under climate scenarios SSP1-2.6 and SSP2-4.5. Furthermore, flood extent increased by 41% due to coral degradation under climate scenario SSP2-4.5 in 2050. Both the large differences in projected coastal flooding between the climate scenarios, and the potential impact of coral reef degradation on coastal flooding, implies the necessity of limiting the effects of climate change for the future generations on Bonaire.

Lastly, elevation measurements on the coastline of Kralendijk made it possible to validate the global DEM that was used in the model simulations. Compared to the observations, the DEM showed an overestimation of 1.2 metres. When the DEM was corrected for this overestimation, flood extent increased with 94% for the SSP1-2.6 scenario in 2050. This amplifies the need for a high quality DEM for more accurate coastal inundation modelling on Bonaire. Therefore, it is advised to rerun the model simulations when high quality DEM becomes available.

References

Andersen O. B, Knudsen P (2009) The DNSC08 mean sea surface and mean dynamic topography. *J. Geophys. Res., 114*, C11, doi:10.1029/2008JC005179, 2009

Athif, A. A. (2020). *Computationally efficient modelling of wave driven flooding in Atoll Islands* [Investigation on the use of a reduced-physics model solver SFINCS].

Baertz, A. (2022). *NON-ECONOMIC LOSS AND DAMAGE FROM CLIMATE CHANGE ON BONAIRE: An Assessment of the Impacts of Climate Change on Public Health and Cultural Heritag*e [Master thesis, Vrije Universiteit].

Balasubramanian, A. (2017). Digital elevation model (DEM) in GIS. *University of Mysore*.4

Barnard, P. L., Erikson, L. H., Foxgrover, A. C., Hart, J. A. F., Limber, P., O'Neill, A. C., ... & Jones, J. M. (2019). Dynamic flood modeling essential to assess the coastal impacts of climate change. *Scientific reports*, *9*(1), 1–13.

Bloemendaal, N., de Moel, H., Martinez, A. B., Muis, S., Haigh, I. D., van der Wiel, K.,& Aerts, J. C. (2022). A globally consistent local-scale assessment of future tropical cyclone risk. *Science advances*, *8*(17), eabm8438.

Bloemendaal, N., Haigh, I. D., de Moel, H., Muis, S., Haarsma, R. J., & Aerts, J. C. (2020). Generation of a global synthetic tropical cyclone hazard dataset using STORM. *Scientific Data*, *7*(1), 1–12.

Buchhorn, M., Smets, B., Bertels, L., De Roo, B., Lesiv, M., Tsendbazar, N. - E., Herold, M., Fritz, S. Copernicus Global Land Service: Land Cover 100m: collection 3: epoch 2019: Globe 2020. DOI 10.5281/zenodo.3939050

Buijs, S.L. (2022). *Protecting Bonaire against coastal flooding: a participatory multi-criteria analysis of coastal adaptation strategies.* Master thesis, Vrije Universiteit Amsterdam.

Cha, E. J., Knutson, T. R., Lee, T. C., Ying, M., & Nakaegawa, T. (2020). Third assessment on impacts of climate change on tropical cyclones in the Typhoon Committee Region–Part II: Future projections. *Tropical Cyclone Research and Review*, *9*(2), 75-86.

Climate Studies Group Mona (Eds.). 2020. "*The State of the Caribbean Climate*". Produced for the Caribbean Development Bank. http://dx.doi.org/10.13140/RG.2.2.16732.92808

Danard, M., Munro, A., & Murty, T. (2003). Storm surge hazard in Canada. *Natural Hazards*, *28*(2), 407-434.

DCBD. (2022, June 25). Elevation and coastal bathymetric model for Bonaire. https://www.dcbd.nl/document/elevation-and-coastal-bathymetric-model-bonaire

De Boer, M.N. (2022). *The vulnerable future of Bonaire: A direct climate damage assessment of the buildings and critical infrastructure of Bonaire*. Master thesis, Vrije Universiteit Amsterdam.

De Laat, J. (2022, June 29). *Tropische orkanen bij benedenwindse eilanden: geen ABC-tje*. *KNMI.* https://www.knmi.nl/over-het-knmi/nieuws/tropische-orkanen-bij-benedenwindse-eilanden-geen-abc-tje

Dullaart, J. (2022). *Enabling dynamic modelling of global coastal flooding by defining storm tide hydrographs*. [Unpublished manuscript]

Dullaart, J., Muis, S., Bloemendaal, N., Chertova, M. V., Couasnon, A., & Aerts, J. C. (2021). Accounting for tropical cyclones more than doubles the global population exposed to low-probability coastal flooding. *Communications Earth & Environment*, *2*(1), 1–11.

Eilander, Dirk, Leijnse, Tim, & Winsemius, Hessel C. (2022). hydroMT-sfincs (v0.2.1). Zenodo. https://doi.org/10.5281/zenodo.6244556

Ferrario, F., Beck, M. W., Storlazzi, C. D., Micheli, F., Shepard, C. C., & Airoldi, L. (2014). The effectiveness of coral reefs for coastal hazard risk reduction and adaptation. *Nature communications*, *5*(1), 1–9.

Fox-Kemper, B., H.T. Hewitt, C. Xiao, G. Aðalgeirsdóttir, S.S. Drijfhout, T.L. Edwards, N.R. Golledge, M. Hemer, R.E. Kopp, G. Krinner, A. Mix, D. Notz, S. Nowicki, I.S. Nurhati, L. Ruiz, J.-B. Sallée, A.B.A. Slangen, and Y. Yu (2021). Ocean, Cryosphere and Sea Level Change. In MassonDelmotte, V., P. Zhai, A. Pirani, S.L. Connors, C. Péan, S. Berger, N. Caud, Y. Chen, L. Goldfarb, M.I. Gomis, M. Huang, K. Leitzell, E. Lonnoy, J.B.R. Matthews, T.K. Maycock, T. Waterfield, O. Yelekçi, R. Yu, and B. Zhou (eds.), *Climate Change 2021: The Physical Science Basis. Contribution of Working Group I to the Sixth Assessment Report of the Intergovernmental Panel on Climate Change*. Cambridge University Press. In Press.

Gattuso, J.-P., O. Hoegh-Guldberg, and H.-O. Pörtner (2014). Cross-chapter box on coral reefs. In Field, C.B., V.R. Barros, D.J. Dokken, K.J. Mach, M.D. Mastrandrea, T.E. Bilir, M. Chatterjee, K.L. Ebi, Y.O. Estrada, R.C. Genova, B. Girma, E.S. Kissel, A.N. Levy, S. MacCracken, P.R. Mastrandrea, and L.L. White (eds.), *Climate Change 2014: Impacts, Adaptation, and Vulnerability. Part A: Global and Sectoral Aspects. Contribution of Working Group II to the Fifth Assessment Report of the Intergovernmental Panel on Climate Change* (pp. 97–100). Cambridge, United Kingdom and New York, NY, USA: Cambridge University Press.

GEBCO Compilation Group (2021) GEBCO 2021 Grid (doi:10.5285/c6612cbe-50b3-0cff-e053-6c86abc09f8f

Geomaat Caribe B.V., personal communication, (May 24, 2022).

Guza, R. T., & Thornton, E. B. (1981). Wave set-up on a natural beach. *Journal of Geophysical Research: Oceans*, *86*(C5), 4133-4137.

Harley, M. (2017). Coastal storm definition. *Coastal storms: Processes and impacts*, 1–21.

Hawker, L., Uhe, P., Paulo, L., Sosa, J., Savage, J., Sampson, C., & Neal, J. (2022). A 30m global map of elevation with forests and buildings removed. *Environmental Research Letters*.

Hersbach, H., Bell, B., Berrisford, P., Biavati, G., Horányi, A., Muñoz Sabater, J., Nicolas, J., Peubey, C., Radu, R., Rozum, I., Schepers, D., Simmons, A., Soci, C., Dee, D., Thépaut, J-N. (2018). *ERA5 hourly data on single levels from 1979 to present*. Copernicus Climate Change Service (C3S) Climate Data Store (CDS). (Accessed on 14-04-2022), 10.24381/cds.adbb2d47

Hersbach, H., Bell, B., Berrisford, P., Hirahara, S., Horányi, A., Muñoz-Sabater, J., & Thépaut, J. N. (2020). The ERA5 global reanalysis. *Quarterly Journal of the Royal Meteorological Society*, *146*(730), 1999–2049.

Hoegh-Guldberg, O. (2011). The impact of climate change on coral reef ecosystems. In *Coral reefs: an ecosystem in transition* (pp. 391-403). Dordrecht: Springer.

Hughes, M. (2016). Coastal waves, water levels, beach dynamics and climate change. *Coast Adapt, National Climate Change Adaptation Research Facility, Gold Coast*.

IPCC, 2013: Climate Change 2013: The Physical Science Basis. Contribution of Working Group I to the Fifth Assessment Report of the Intergovernmental Panel on Climate Change [Stocker, T.F., D. Qin, G.-K. Plattner, M. Tignor, S.K. Allen, J. Boschung, A. Nauels, Y. Xia, V. Bex and P.M. Midgley (eds.)]. Cambridge University Press, Cambridge, United Kingdom and New York, NY, USA, 1535 pp.

IPCC, 2021: Climate Change 2021: The Physical Science Basis. Contribution of Working Group I to the Sixth Assessment Report of the Intergovernmental Panel on Climate Change [Masson-Delmotte, V., P. Zhai, A. Pirani, S.L. Connors, C. Péan, S. Berger, N. Caud, Y. Chen, L. Goldfarb, M.I. Gomis, M. Huang, K. Leitzell, E. Lonnoy, J.B.R. Matthews, T.K. Maycock, T. Waterfield, O. Yelekçi, R. Yu, and B. Zhou (eds.)]. Cambridge University Press. In Press.

Jaafar, Hadi; Ahmad, Farah (2019). *GCN250, global curve number datasets for hydrologic modeling and design. figshare*. Dataset. https://doi.org/10.6084/m9.figshare.7756202.v1

Johnson, H. K. (2006). Wave modelling in the vicinity of submerged breakwaters. *Coastal engineering*, *53*(1), 39–48.

Kim, S. Y., Yasuda, T., & Mase, H. (2010). Wave set-up in the storm surge along open coasts during Typhoon Anita. *Coastal Engineering*, *57*(7), 631–642.

Koninklijk Nederlands Meteorologisch Instituut 2021. *KNMI Klimaatsignaal'21. Hoe het klimaat in Nederland snel verandert. https://cdn.knmi.nl/knmi/asc/klimaatsignaal21/KNMI_Klimaatsignaal21.pdf*

Kulp, S. A., & Strauss, B. H. (2018). CoastalDEM: A global coastal digital elevation model improved from SRTM using a neural network. *Remote sensing of environment*, *206*, 231–239.

L.A. Nurse, R.F. Mclean, J. Agard, L.P. Briguglio, V. Duvat-Magnan, *et al.* (2014). Small islands. Barros, V.R., C.B. Field, D.J. Dokken, M.D. Mastrandrea, K.J. Mach, T.E. Bilir, M. Chatterjee, K.L. Ebi, Y.O. Estrada, R.C. Genova, B. Girma, E.S. Kissel, A.N. Levy, S. MacCracken, P.R. Mastrandrea, & L.L. White (eds.). *Climate Change 2014: Impacts, Adaptation, and Vulnerability. Part B: Regional Aspects. Contribution of Working Group II to the Fifth Assessment Report of the Intergovernmental Panel on Climate Change* (pp. 1613–1654). Cambridge University Press. ffhal-01090732

Le Bars, D., De Vries, H., & Drijfhout, S. (2019). *Sea level rise and its spatial variations*. De Bilt, Technical Report, 372.

Leijnse, T. (2018). Computationally Efficient Modelling of Compound Flooding due to Tropical Cyclones with the Explicit Inclusion of Wave-Driven Processes: Research into the required processes and the implementation within the SFINCS model.

Leijnse, T. (2022). SFINCS Documentation. Retrieved from: https://sfincs.readthedocs.io/_/downloads/en/latest/pdf/

Leon, J. X., Heuvelink, G. B., & Phinn, S. R. (2014). Incorporating DEM uncertainty in coastal inundation mapping. *PLoS one*, *9*(9), e108727.

Lugo-Fernández, A., & Roberts, H. H. (2011). *Reef front wave energy*.

Massel, S. R., & Gourlay, M. R. (2000). On the modelling of wave breaking and set-up on coral reefs. *Coastal engineering*, *39*(1), 1–27.

McClean, F., Dawson, R., & Kilsby, C. (2020). Implications of using global digital elevation models for flood risk analysis in cities. *Water Resources Research*, *56*(10), e2020WR028241.

Mélice, J. L., & Reason, C. J. (2007). Return period of extreme rainfall at George, South Africa. *South African Journal of science*, *103*(11–12), 499–501.

Meteorological Department of Curaçao (2016) URL: http://www.meteo.cw/climate.php?Lang=Eng&St=TNCC&Sws=R11

Mücher, S., Suomalainen, J., Stuiver, J., & Meesters, E. (2017). *Hyperspectral Coral Reef Classification of Bonaire* (No. C062/17). Wageningen Marine Research.

Muis, S., Apecechea, M. I., Dullaart, J., de Lima Rego, J., Madsen, K. S., Su, J., ... & Verlaan, M. (2020). A high-resolution global dataset of extreme sea levels, tides, and storm surges, including future projections. *Frontiers in Marine Science*, *7*, 263.

Muis, S., Verlaan, M., Winsemius, H. C., Aerts, J. C., & Ward, P. J. (2016). A global reanalysis of storm surges and extreme sea levels. *Nature communications*, *7*(1), 1–12.

Myers, V. A. (1975). *Storm tide frequencies on the South Carolina Coast* (Vol. 16). Office of Hydrology, National Weather Service.

Nasa, Sea Level Change (2022, March 30). Projected Sea-Level Rise Under Different SSP Scenarios. https://sealevel.nasa.gov/ipcc-ar6-sea-level-projection-tool?lat=12&lon=-69

O'Neill, B. C., Carter, T. R., Ebi, K., Harrison, P. A., Kemp-Benedict, E., Kok, K., ... & Pichs-Madruga, R. (2020). Achievements and needs for the climate change scenario framework. *Nature climate change*, *10*(12), 1074–1084.

Oppenheimer, M., B.C. Glavovic , J. Hinkel, R. van de Wal, A.K. Magnan, A. Abd-Elgawad, R. Cai, M. Cifuentes-Jara, R.M. DeConto, T. Ghosh, J. Hay, F. Isla, B. Marzeion, B. Meyssignac, and Z. Sebesvari (2019). Sea Level Rise and Implications for Low-Lying Islands, Coasts and Communities. In H.-O. Pörtner, D.C. Roberts, V. Masson-Delmotte, P. Zhai, M. Tignor, E. Poloczanska, K. Mintenbeck, A. Alegría, M. Nicolai, A. Okem, J. Petzold, B. Rama, N.M. Weyer (eds.), I*PCC Special Report on the Ocean and Cryosphere in a Changing Climate*. In press.

Palanisamy, H., Becker, M., Meyssignac, B., Henry, O., & Cazenave, A. (2012). Regional sea level change and variability in the Caribbean Sea since 1950. *Journal of Geodetic Science*, *2*(2), 125-133.

PDOK. (2022, June 28). Dataset: Actueel Hoogtebestand Nederland (AHN3). https://www.pdok.nl/introductie/-/article/actueel-hoogtebestand-nederland-ahn3-

Peachey, D. R. (1986). Modeling waves and surf. *ACM Siggraph Computer Graphics*, *20*(4), 65-74.

Péquignet, A. C. N., Becker, J. M., & Merrifield, M. A. (2014). Energy transfer between wind waves and low-frequency oscillations on a fringing reef, I pan, G uam. *Journal of Geophysical Research: Oceans*, *119*(10), 6709-6724.

Petit, J. & G. Prudent (2008). *Climate Change and Biodiversity in the European Union Overseas Entities*. IUCN, Brussels, 178pp.

Poulter, B., & Halpin, P. N. (2008). Raster modelling of coastal flooding from sea-level rise. *International Journal of Geographical Information Science*, *22*(2), 167–182.

Pugh, D. (2004). *Changing sea levels: effects of tides, weather and climate*. Cambridge University Press.

Scheffers, A., & Scheffers, S. (2006). Documentation of the impact of Hurricane Ivan on the coastline of Bonaire (Netherlands Antilles). *Journal of Coastal Research*, *22*(6), 1437–1450.

Schep, S., van Beukering, P., Brander, L., & Wolfs, E. (2013). *The tourism value of nature on Bonaire*.

Schmid, K., Hadley, B., & Waters, K. (2014). Mapping and portraying inundation uncertainty of bathtub-type models. *Journal of Coastal Research*, *30*(3), 548–561.

Schmutz, P. P., Potter, A. E., & Arnold Modlin, E. (2017). Aruba, Bonaire, and Curaçao. In *Landscapes and landforms of the Lesser Antilles* (pp. 293–317). Springer, Cham.

Sebastian, A., Bader, D. J., Nederhoff, C. M., Leijnse, T. W. B., Bricker, J. D., & Aarninkhof, S. G. J. (2021). Hindcast of pluvial, fluvial, and coastal flood damage in Houston, Texas during Hurricane Harvey (2017) using SFINCS. *Natural hazards*, *109*(3), 2343–2362.

Seneviratne, S.I., X. Zhang, M. Adnan, W. Badi, C. Dereczynski, A. Di Luca, S. Ghosh, I. Iskandar, J. Kossin, S. Lewis, F. Otto, I. Pinto, M. Satoh, S.M. Vicente-Serrano, M. Wehner, & B. Zhou (2021). Weather and Climate Extreme Events in a Changing Climate. In MassonDelmotte, V., P. Zhai, A. Pirani, S.L. Connors, C. Péan, S. Berger, N. Caud, Y. Chen, L. Goldfarb, M.I. Gomis, M. Huang, K. Leitzell, E. Lonnoy, J.B.R. Matthews, T.K. Maycock, T. Waterfield, O. Yelekçi, R. Yu, and B. Zhou (eds.), *Climate Change 2021: The Physical Science Basis. Contribution of Working Group I to the Sixth Assessment Report of the Intergovernmental Panel on Climate Change*. Cambridge University Press. In Press.

Sheppard, C., Dixon, D. J., Gourlay, M., Sheppard, A., & Payet, R. (2005). Coral mortality increases wave energy reaching shores protected by reef flats: examples from the Seychelles. *Estuarine, Coastal and Shelf Science*, *64*(2-3), 223–234.

Simpson, M., Scott, D., & Trotz, U. (2011). Climate change's impact on the Caribbean's ability to sustain tourism, natural assets, and livelihoods. *Inter-American Development Bank, Washington, DC*.

Statistics Netherlands. (2021). *Trends in the Caribbean Netherlands 2021*. https://longreads.cbs.nl/ticn2021/bonaire/

Steneck, R. S., Arnold, S. N., Boenish, R., De León, R., Mumby, P. J., Rasher, D. B., & Wilson, M. W. (2019). Managing recovery resilience in coral reefs against climate-induced bleaching and hurricanes: a 15 year case study from Bonaire, Dutch Caribbean. *Frontiers in Marine Science*, *6*, 265.

Stephenson, T. S., & Jones, J. J. (2017). Impacts of climate change on extreme events in the coastal and marine environments of Caribbean Small Island Developing States (SIDS). *Caribbean Marine Climate Change Report Card: Science Review*, *2017*, 10–22.

Tait, R. J. (1972). Wave set-up on coral reefs. *Journal of Geophysical Research*, *77*(12), 2207–2211.

Taylor, M. A., Clarke, L. A., Centella, A., *et al.* (2018). Future Caribbean climates in a world of rising temperatures: the 1.5 vs 2.0 dilemma. *Journal of Climate*, *31*(7), 2907–2926.

Thomas, T. J., & Dwarakish, G. S. (2015). Numerical wave modelling–A review. *Aquatic procedia*, *4*, 443–448.

Tide schedule in Bonaire in the Netherlands Antilles. (2022, May 10). Seatemperatu.eu. https://www.seatemperatu.re/caribbean/netherlands-antilles/bonaire/tides.html

Torres, R. R., & Tsimplis, M. N. (2011). Tides and long-term modulations in the Caribbean Sea. *Journal of Geophysical Research: Oceans*, *116*(C10).

Torres, R. R., & Tsimplis, M. N. (2013). Sea-level trends and interannual variability in the Caribbean Sea. *Journal of Geophysical Research: Oceans*, *118*(6), 2934–2947.

van der Knaap, M.E.J.R. (2022). *Reef degradation and Tourism: The macroeconomic costs of climate change on Bonaire.* Master thesis, Vrije Universiteit Amsterdam.

van der Lely, J. A. C., van Beukering, P., Muresan, L., Cortes, D. Z., Wolfs, E., & Schep, S. (2013). *The total economic value of nature on Bonaire*. IVM report (R-13/01). Institute for Environmental Studies, Vrije Universiteit Amsterdam.

van Vuuren, D. P., & Carter, T. R. (2014). Climate and socio-economic scenarios for climate change research and assessment: reconciling the new with the old. *Climatic change*, *122*(3), 415–429.

van Zee, R. (2022). Hydraulic circulation of the tides in Lac Bay, Bonaire. *Isla*, *13*, 05–2012.

Verweij, P., Cormont, A., Nel, J., de Rooij, B., Jones-Walters, L., Slijkerman, D., ... & Teles, I. D. (2020). *A nature inclusive vision for Bonaire in 2050* (No. 3023). Wageningen Environmental Research.

Vousdoukas, M. I., Mentaschi, L., Voukouvalas, E., Verlaan, M., Jevrejeva, S., Jackson, L. P., & Feyen, L. (2018). Global probabilistic projections of extreme sea levels show intensification of coastal flood hazard. *Nature communications*, *9*(1), 1–12.

Vousdoukas, M.I., Voukouvalas, E., Mentaschi, L., Dottori, F., Giardino, A., Bouziotas, D., Bianchi, A., Salamon, P., Feyen, L., 2016. Developments in large-scale coastal flood hazard mapping. Nat. Hazards Earth Syst. Sci. 16, 1841–1853. https://doi.org/10.5194/nhess-16-1841-2016.

Wahl, T., Jain, S., Bender, J., Meyers, S. D., & Luther, M. E. (2015). Increasing risk of compound flooding from storm surge and rainfall for major US cities. *Nature Climate Change*, *5*(12), 1093–1097.

Weaver, R. J., & Slinn, D. N. (2010). Influence of bathymetric fluctuations on coastal storm surge. *Coastal engineering*, *57*(1), 62–70.

Wilkinson, C. R. (1996). Global change and coral reefs: impacts on reefs, economies and human cultures. *Global Change Biology*, *2*(6), 547–558.

Williams, L. L., & Lück-Vogel, M. (2020). Comparative assessment of the GIS based bathtub model and an enhanced bathtub model for coastal inundation. *Journal of Coastal Conservation*, *24*(2), 1–15.

Yamazaki, D., Ikeshima, D., Sosa, J., Bates, P. D., Allen, G. H., & Pavelsky, T. M. (2019). MERIT Hydro: A high-resolution global hydrography map based on latest topography dataset. Water Resources Research, 55(6), 5053–5073.

Yunus, A. P., Avtar, R., Kraines, S., Yamamuro, M., Lindberg, F., & Grimmond, C. S. B. (2016). Uncertainties in tidally adjusted estimates of sea level rise flooding (bathtub model) for the greater London. *Remote Sensing*, *8*(5), 366

Annex A Configuration file (.ini)

File Edit Format View Help

```
[global]
write_gis = True                # write addtional geotif and geojson files to gis subfolder
config_fn = sfincs.inp          # name of sfincs config (inp) file

[setup_config]
tref = 20000101 000000
tstart = 20000101 000000
tstop = 20000107 045000
dtout = 600
alpha = 0.5
zsini = 0.5

[setup_topobathy]
topobathy_fn = fab_dem          #DEM
crs = utm                       # model CRS (must be UTM zone)

[setup_merge_topobathy]
topobathy_fn = gebco            # bathymetry ['elevtn']
mask_fn = osm_coastlines        # sea polygon
offset_fn = dtu10mdt_egm96      # mean dynamic topography
merge_buffer = 2                # buffer (cells) between elevation and bathymetry data filled with 'linear' interpolation
merge_method=first

[setup_mask]
elv_min = -5                    # minimum elevation for valid cells
exclude_mask_fn = osm_coastlines        #sets coastline

[setup_cn_infiltration]
cn_fn = gcn250                  # curve number source
antecedent_runoff_conditions = avg # for gcn250: {'dry', 'avg', 'wet'}

[setup_manning_roughness]
lulc_fn = vito                  # land-use land-cover source
map_fn = None                   # mapping file. read from hydromt/data/lulc/{lulc_fn}_mapping.csv if None

[setup_bounds]
btype = waterlevel              # boundary type ['waterlevel', 'outflow']
include_mask_fn = osm_coastlines  # sea polygon

[setup_h_forcing]
geodataset_fn = hydrographs     # waterlevel timeseries dataset. see local data_sources.yml file
buffer = 1e4                    # buffer around model region to select gauges
```

Annex B Data catalogue File (.yml)

File Edit Format View Help


```yaml
dtu10mdt_egm96:
  crs: 4326
  data_type: RasterDataset
  driver: raster
  meta:
    category: topography
    paper_doi: 10.1029/2008JC005179
    paper_ref: Andersen and Knudsen (2009)
    source url: https://www.space.dtu.dk/english/research/scientific data and models/global mean dynamic topography
    source_version: 2010
    unit: m+EGM96
  path: dtu10mdt_egm96.tif
gcn250:
  data_type: RasterDataset
  driver: raster
  meta:
    category: soil
    paper_doi: 10.1038/s41597-019-0155-x
    paper_ref: Jaafar et al. (2019)
    source_license: CC BY 4.0
    source_url: https://doi.org/10.6084/m9.figshare.7756202.v1
    source_version: v1
  nodata: 255
  path: gcn250\{variable}.tif
gebco:
  crs: 4326
  data_type: RasterDataset
  driver: raster
  meta:
    category: topography
    paper_doi: 10.5285/a29c5465-b138-234d-e053-6c86abc040b9
    paper_ref: Weatherall et al (2020)
    source_license: https://www.gebco.net/data_and_products/gridded_bathymetry_data/#a1
    source url: https://www.bodc.ac.uk/data/open download/gebco/gebco 2020/geotiff/
    source_version: 2020
    unit: m+MSL
  path: gebco.tif
grwl_mask:
  data_type: RasterDataset
  driver: raster
  meta:
    category: hydrography
    paper_doi: 10.1126/science.aat0636
    paper ref: Allen and Pavelsky (2018)
    source_license: CC BY 4.0
    source_url: https://doi.org/10.5281/zenodo.1297434
    source_version: 1.01
  nodata: 0
  path: grwl_mask.tif
mdt_cnes_cls18:
  crs: 4326
  data_type: RasterDataset
  driver: raster
  meta:
    category: topography
    paper_doi: 10.5194/os-17-789-2021
    paper_ref: Mulet et al (2021)
    source url: https://www.aviso.altimetry.fr/en/data/products/auxiliary products/mdt.html
    source_version: 18
    unit: m+GOCO05S
  path: mdt_cnes_cls18.tif
merit hydro:
  crs: 4326
  data_type: RasterDataset
  driver: raster
  meta:
    category: topography
    paper_doi: 10.1029/2019WR024873
    paper ref: Yamazaki et al. (2019)
    source_license: CC-BY-NC 4.0 or ODbL 1.0
    source_url: http://hydro.iis.u-tokyo.ac.jp/~yamadai/MERIT_Hydro
    source_version: 1.0
  path: merit_hydro\{variable}.tif
fab_dem:
  crs: 4326
  data type: RasterDataset
  driver: raster
  meta:
    category:
    paper_doi:
    paper_ref:
    source_license:
    source url:
    source_version:
  path: fab_dem\{variable}.tif
osm_coastlines:
  crs: 4326
  data_type: GeoDataFrame
  driver: vector
  meta:
    category: geography
    source_author: OpenStreetMap
    source_info: OpenStreetMap coastlines water polygons, last updated 2020 01 09T05:29
    source_license: ODbL
    source_url: https://osmdata.openstreetmap.de/data/coastlines.html
    source_version: 1.0
  path: osm coastlines.gpkg
vito:
  crs: 4326
  data_type: RasterDataset
  driver: raster
  meta:
    category: landuse
    paper doi: 10.5281/zenodo.3939038
    paper_ref: Buchhorn et al (2020)
    source_url: https://land.copernicus.eu/global/products/lc
    source_version: v2.0.2
  path: vito.tif
hydrographs:
  crs: 4326
  data type: GeoDataset
  driver: netcdf
  meta:
    category:
    date:
    source:
  path: new_dem_hydrograph_ssp126_2050.nc
```

Annex C SFINCS input file (.inp)

File Edit Format View Help

```
mmax            = 1582
nmax            = 1718
dx              = 20.0
dy              = 20.0
x0              = 559800.0
y0              = 1327720.0
rotation        = 0
epsg            = 32619
inputformat     = bin
outputformat    = net
tref            = 20000101 000000
tstart          = 20000101 000000
tstop           = 20000107 045000
dtout           = 600
dthisout        = 600
dtmaxout        = 86400
advection       = 0
alpha           = 0.5
huthresh        = 0.05
theta           = 0.9
min_lev_hmax    = -1
zsini           = 0.5
depfile         = sfincs.dep
mskfile         = sfincs.msk
indexfile       = sfincs.ind
scsfile         = sfincs.scs
manningfile     = sfincs.man
bzsfile         = sfincs.bzs
bndfile         = sfincs.bnd
inifile         = C:\Users\stanv\OneDrive\Documenten\hydrology\Thesis\SFINCS\restart_ssp585_2150\sfincs.restart
```

Annex D Field elevation measurements

Location	Latitude	Longitude	Observation elevation (m)	FABDEM elevation (m)	Difference (m)	Average difference (m)
1	12.164	-68.284	0.60	1.58	0.98	1.20
2	12.161	-68.283	2.00	3.19	1.19	
3	12.159	-68.281	1.75	3.19	1.44	
4	12.156	-68.279	1.25	2.91	1.66	
5	12.153	-68.278	1.62	2.75	1.13	
6	12.152	-68.278	1.42	3.17	1.75	
7	12.150	-68.277	1.90	2.67	0.77	
8	12.149	-68.277	2.20	2.33	0.13	
9	12.146	-68.276	2.65	2.71	0.06	
10	12.135	-68.270	1.75	2.47	0.72	
11	12.135	-68.278	2.15	2.80	0.65	
12	12.132	-68.249	3.11	4.61	1.50	
13	12.153	-68.273	2.728	3.37	0.64	
14	12.138	-68.253	4.89	6.9	2.01	
15	12.186	-68.264	18.84	20.69	1.85	
16	12.186	-68.264	16.94	19.68	2.74	

Annex E Bathtub inundation maps of 2050, 2100, 2150 and 2300

2050:

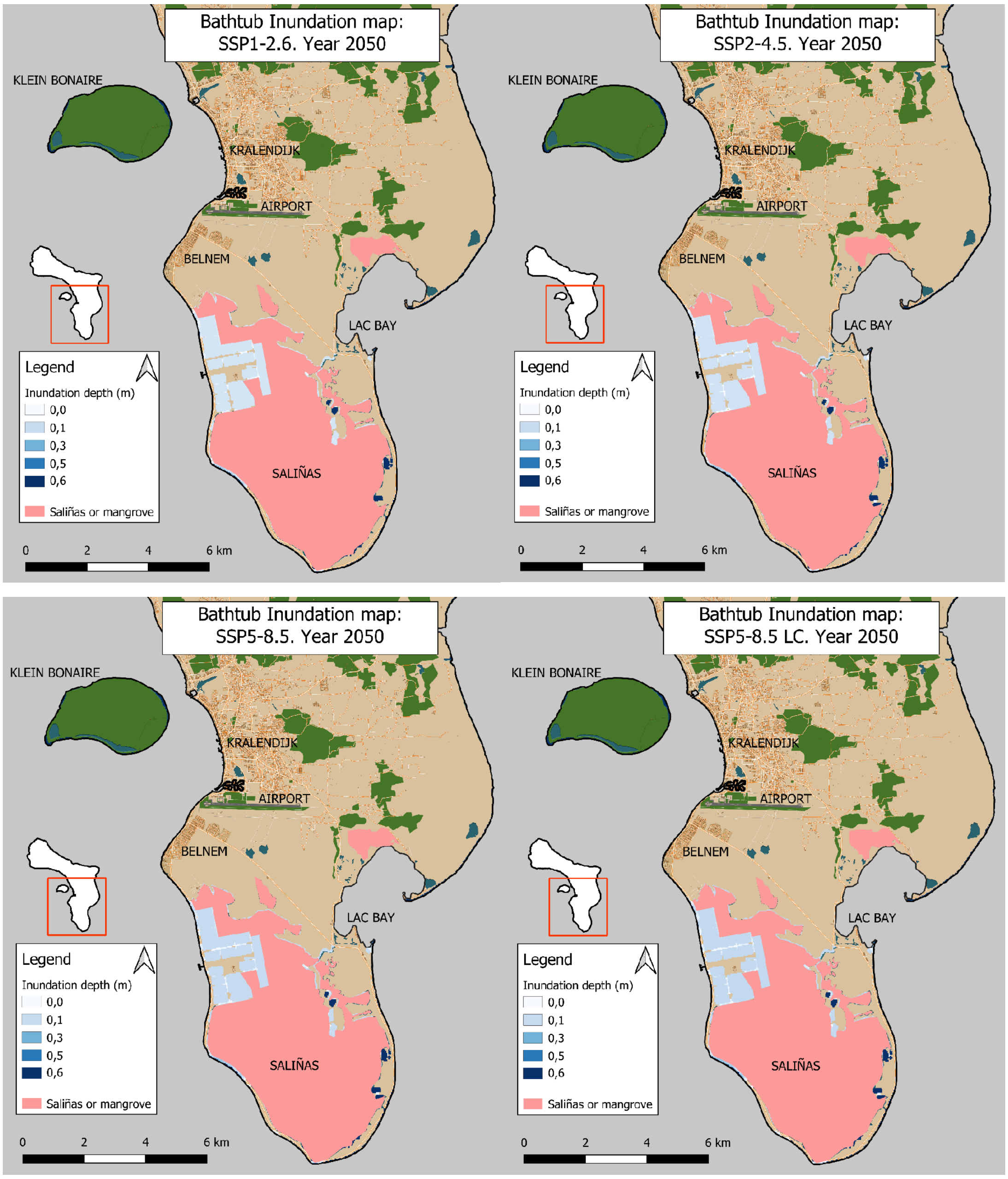

2100:

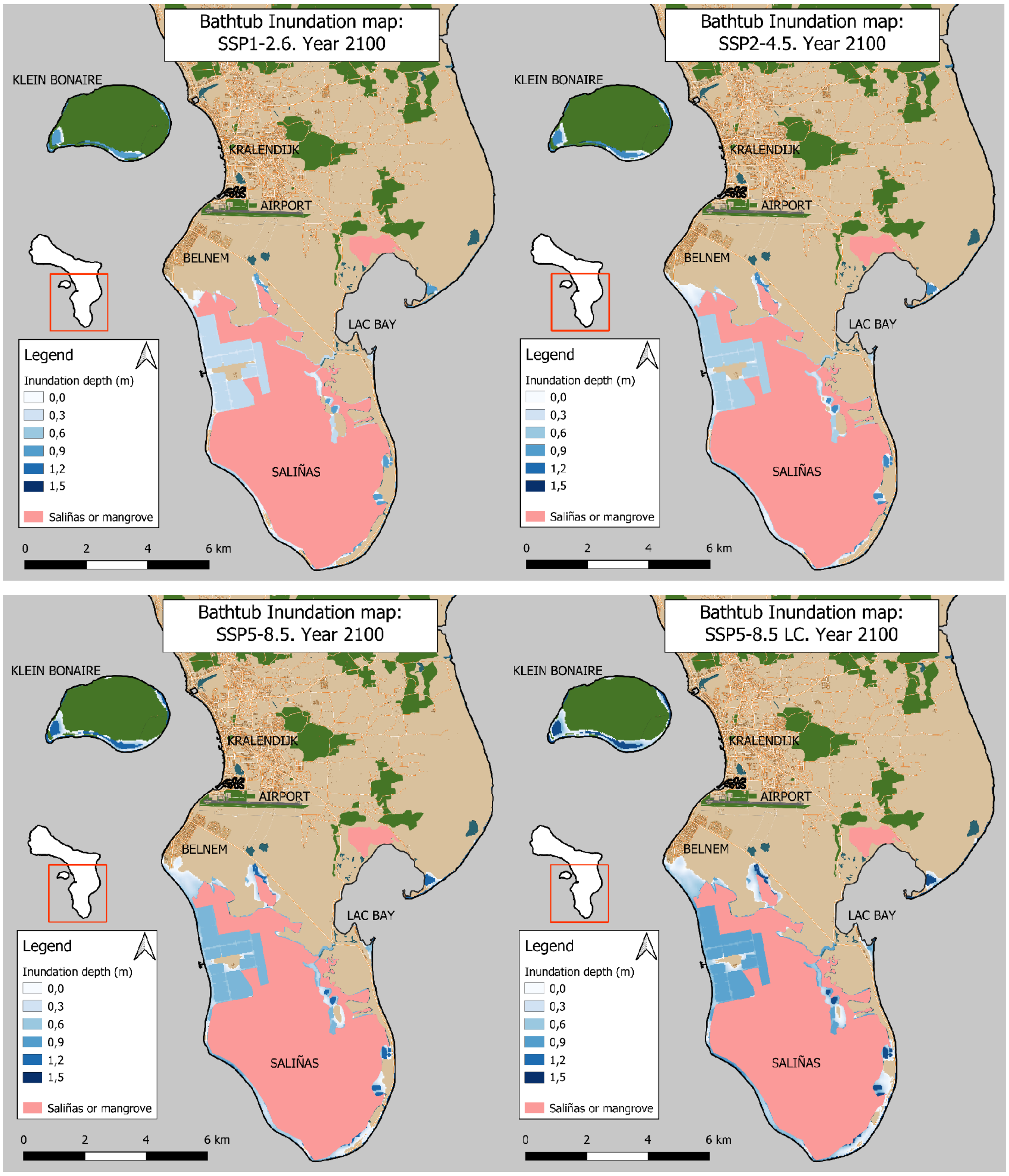
Bathtub Inundation map:
SSP1-2.6. Year 2100
KLEIN BONAIRE
KRALENDIJK
AIRPORT
BELNEM
LAC BAY
SALIÑAS
Legend
Inundation depth (m)
0,0
0,3
0,6
0,9
1,2
1,5
Saliñas or mangrove
0
2
4
6 km
Bathtub Inundation map:
SSP2-4.5. Year 2100
KLEIN BONAIRE
KRALENDIJK
AIRPORT
BELNEM
LAC BAY
SALIÑAS
Legend
Inundation depth (m)
0,0
0,3
0,6
0,9
1,2
1,5
Saliñas or mangrove
0
2
4
6 km
Bathtub Inundation map:
SSP5-8.5. Year 2100
KLEIN BONAIRE
KRALENDIJK
AIRPORT
BELNEM
LAC BAY
SALIÑAS
Legend
Inundation depth (m)
0,0
0,3
0,6
0,9
1,2
1,5
Saliñas or mangrove
0
2
4
6 km
Bathtub Inundation map:
SSP5-8.5 LC. Year 2100
KLEIN BONAIRE
KRALENDIJK
AIRPORT
BELNEM
LAC BAY
SALIÑAS
Legend
Inundation depth (m)
0,0
0,3
0,6
0,9
1,2
1,5
Saliñas or mangrove
0
2
4
6 km

2150:

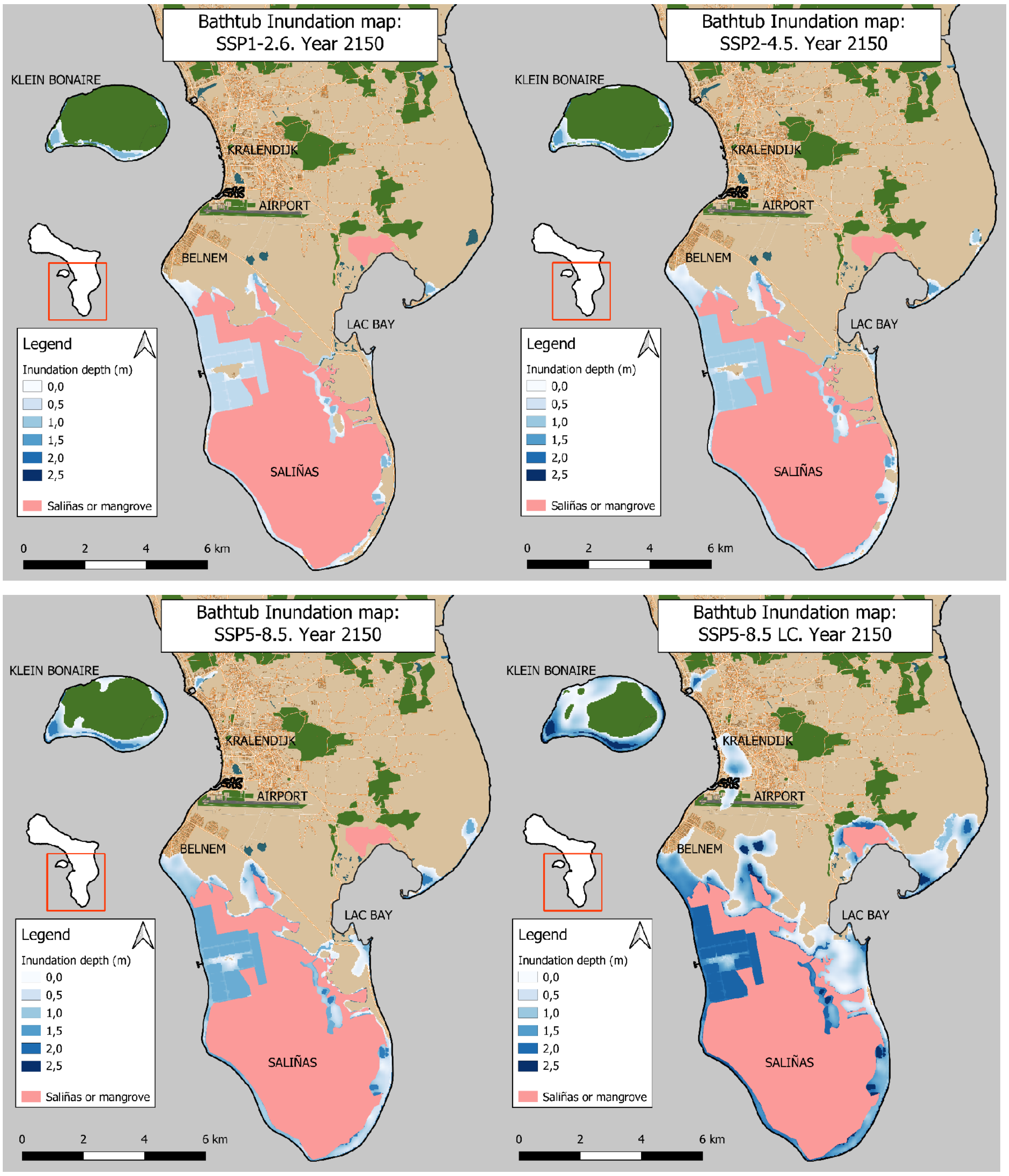
Bathtub Inundation map:
SSP1-2.6. Year 2150
KLEIN BONAIRE
KRALENDIJK
AIRPORT
BELNEM
LAC BAY
SALIÑAS
Legend
Inundation depth (m)
0,0
0,5
1,0
1,5
2,0
2,5
Saliñas or mangrove
0
2
4
6 km
Bathtub Inundation map:
SSP2-4.5. Year 2150
KLEIN BONAIRE
KRALENDIJK
AIRPORT
BELNEM
LAC BAY
SALIÑAS
Legend
Inundation depth (m)
0,0
0,5
1,0
1,5
2,0
2,5
Saliñas or mangrove
0
2
4
6 km
Bathtub Inundation map:
SSP5-8.5. Year 2150
KLEIN BONAIRE
KRALENDIJK
AIRPORT
BELNEM
LAC BAY
SALIÑAS
Legend
Inundation depth (m)
0,0
0,5
1,0
1,5
2,0
2,5
Saliñas or mangrove
0
2
4
6 km
Bathtub Inundation map:
SSP5-8.5 LC. Year 2150
KLEIN BONAIRE
KRALENDIJK
AIRPORT
BELNEM
LAC BAY
SALIÑAS
Legend
Inundation depth (m)
0,0
0,5
1,0
1,5
2,0
2,5
Saliñas or mangrove
0
2
4
6 km

2300:

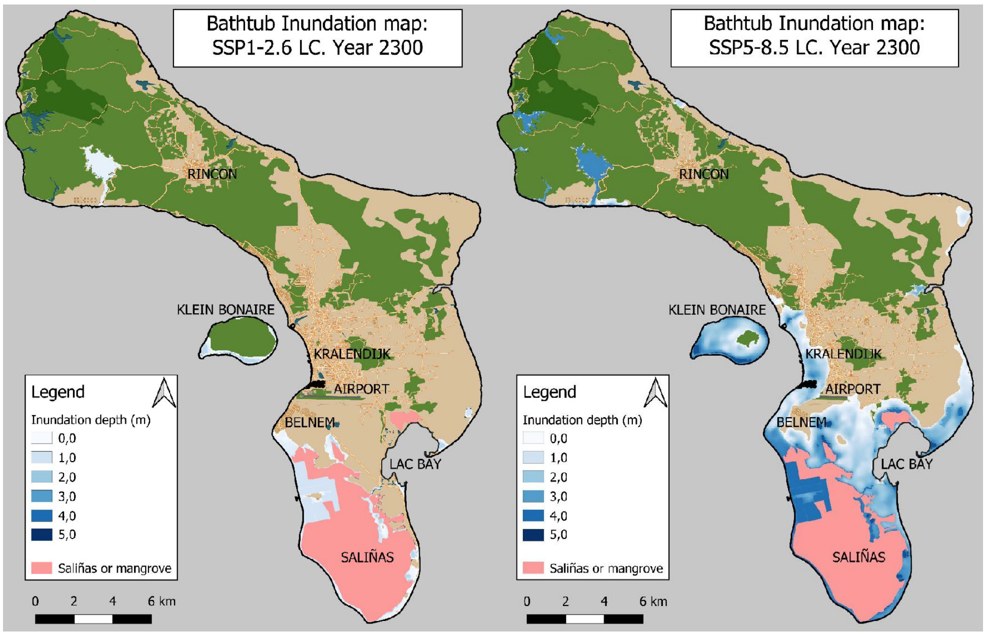
Bathtub Inundation map:
SSP1-2.6 LC. Year 2300
RINCON
KLEIN BONAIRE
KRALENDIJK
AIRPORT
BELNEM
LAC BAY
SALIÑAS
Legend
Inundation depth (m)
0,0
1,0
2,0
3,0
4,0
5,0
Saliñas or mangrove
0 2 4 6 km
Bathtub Inundation map:
SSP5-8.5 LC. Year 2300
RINCON
KLEIN BONAIRE
KRALENDIJK
AIRPORT
BELNEM
LAC BAY
SALIÑAS
Legend
Inundation depth (m)
0,0
1,0
2,0
3,0
4,0
5,0
Saliñas or mangrove
0 2 4 6 km

Annex F SFINCS inundation maps of 2050, 2100, 2150 and 2300

2050:

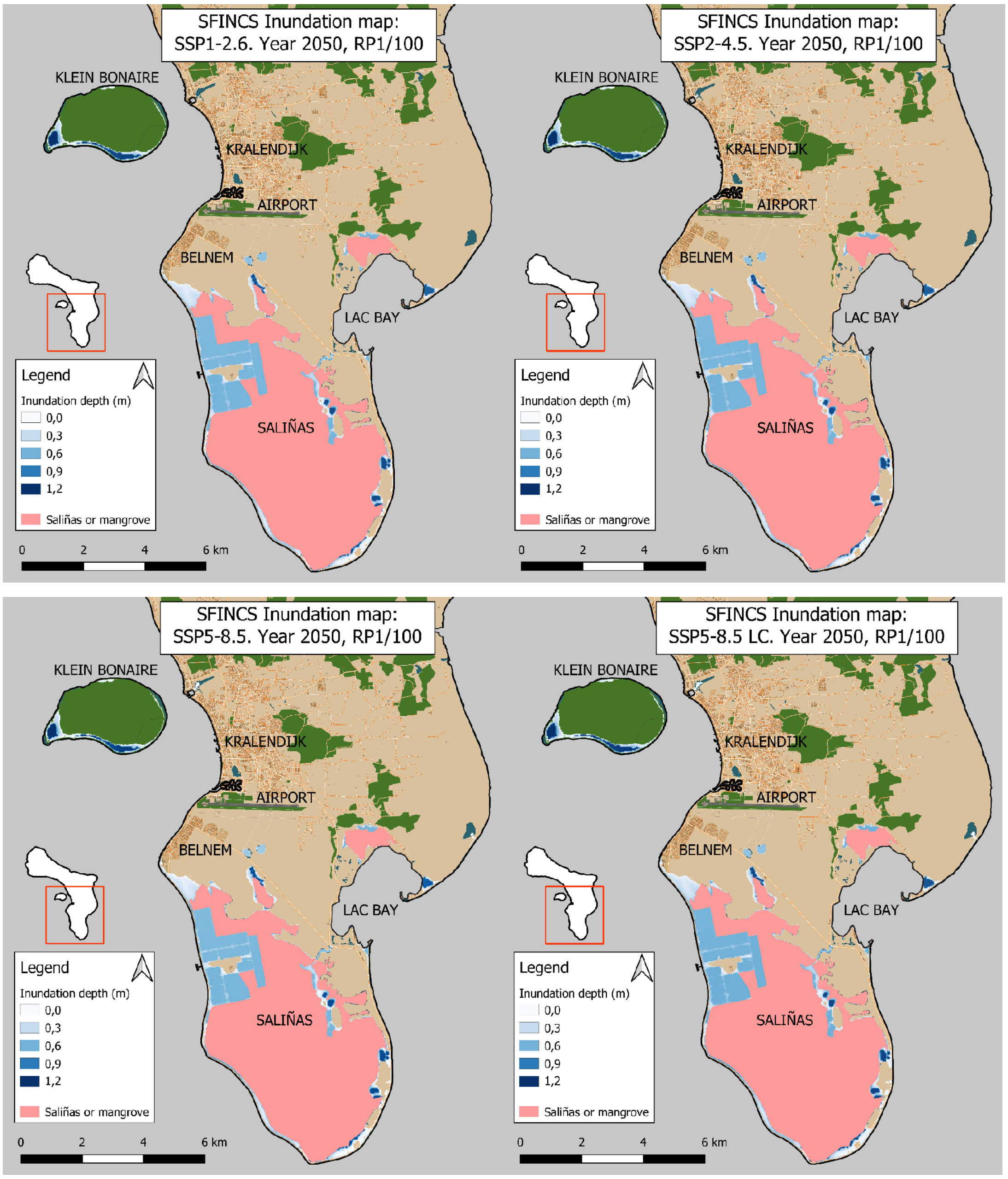

2100:

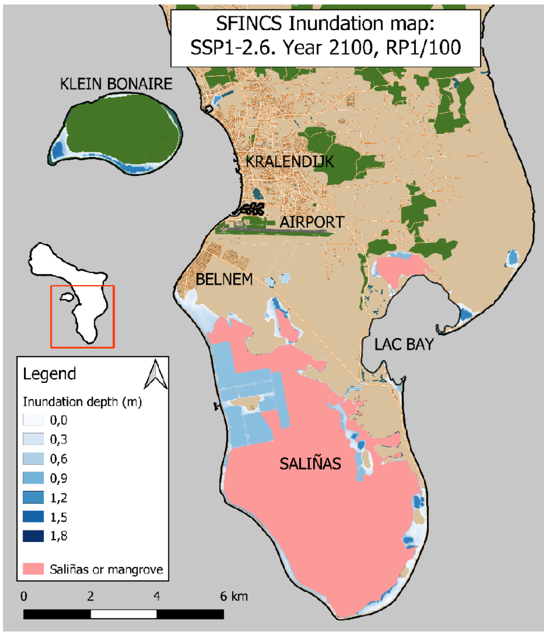
SFINCS Inundation map:
SSP1-2.6. Year 2100, RP1/100
KLEIN BONAIRE
KRALENDIJK
AIRPORT
BELNEM
LAC BAY
SALIÑAS
Legend
Inundation depth (m)
0,0
0,3
0,6
0,9
1,2
1,5
1,8
Saliñas or mangrove
0
2
4
6 km

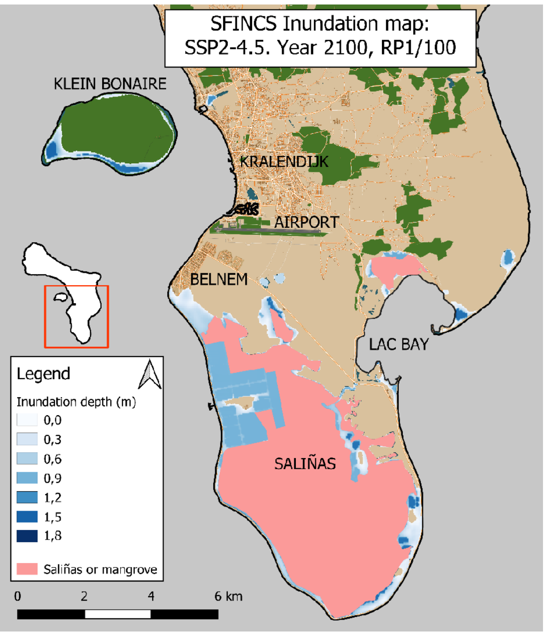
SFINCS Inundation map:
SSP2-4.5. Year 2100, RP1/100
KLEIN BONAIRE
KRALENDIJK
AIRPORT
BELNEM
LAC BAY
SALIÑAS
Legend
Inundation depth (m)
0,0
0,3
0,6
0,9
1,2
1,5
1,8
Saliñas or mangrove
0
2
4
6 km

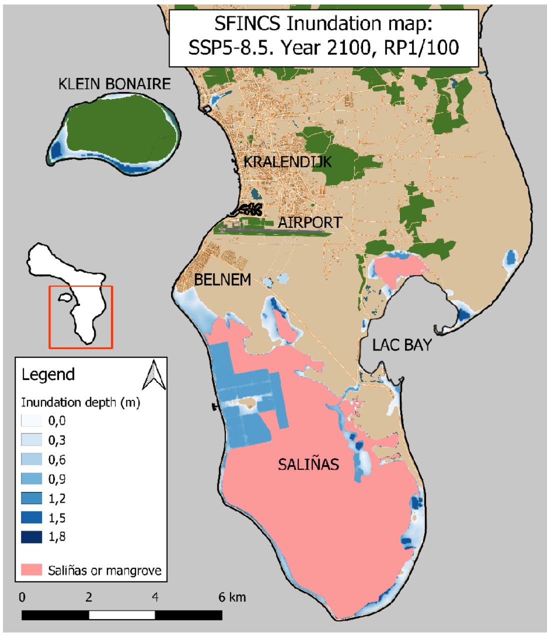
SFINCS Inundation map:
SSP5-8.5. Year 2100, RP1/100
KLEIN BONAIRE
KRALENDIJK
AIRPORT
BELNEM
LAC BAY
SALIÑAS
Legend
Inundation depth (m)
0,0
0,3
0,6
0,9
1,2
1,5
1,8
Saliñas or mangrove
0
2
4
6 km

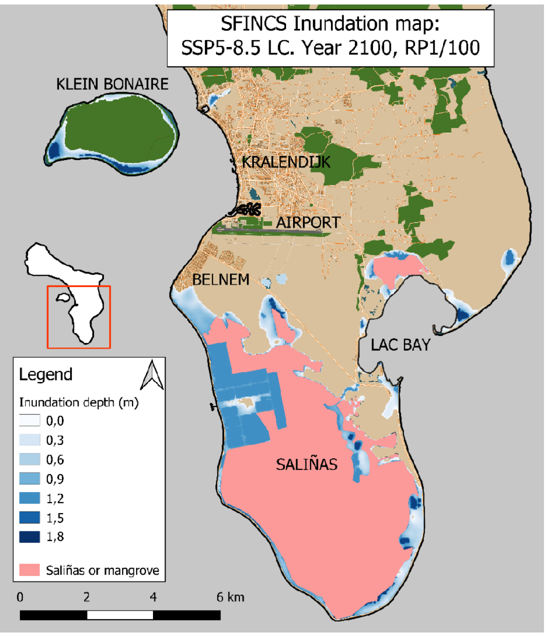
SFINCS Inundation map:
SSP5-8.5 LC. Year 2100, RP1/100
KLEIN BONAIRE
KRALENDIJK
AIRPORT
BELNEM
LAC BAY
SALIÑAS
Legend
Inundation depth (m)
0,0
0,3
0,6
0,9
1,2
1,5
1,8
Saliñas or mangrove
0
2
4
6 km

2150:

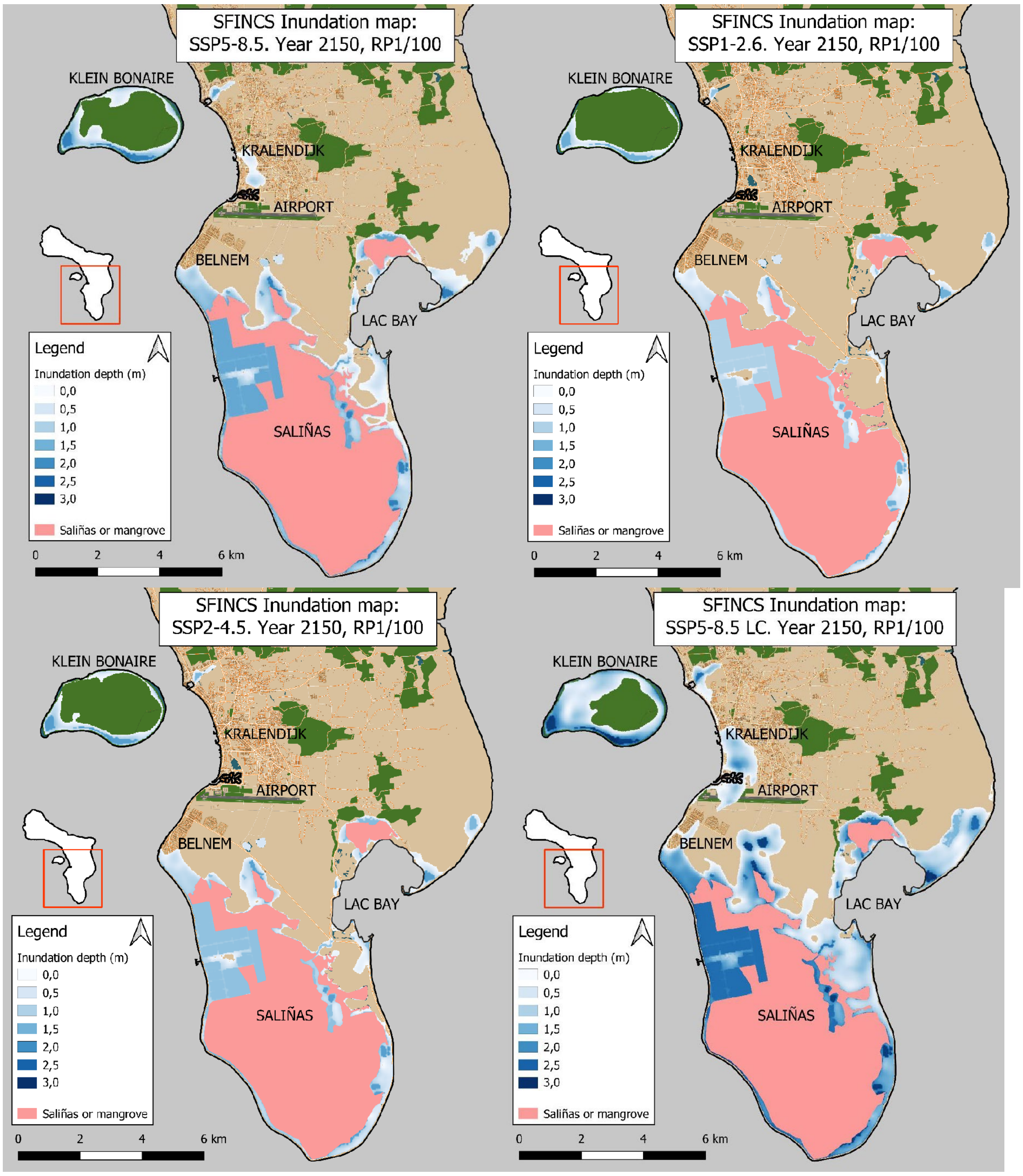
SFINCS Inundation map:
SSP5-8.5. Year 2150, RP1/100
SFINCS Inundation map:
SSP1-2.6. Year 2150, RP1/100
SFINCS Inundation map:
SSP2-4.5. Year 2150, RP1/100
SFINCS Inundation map:
SSP5-8.5 LC. Year 2150, RP1/100
KLEIN BONAIRE
KRALENDIJK
AIRPORT
BELNEM
LAC BAY
SALIÑAS
Legend
Inundation depth (m)
0,0
0,5
1,0
1,5
2,0
2,5
3,0
Saliñas or mangrove
0
2
4
6 km

2300:

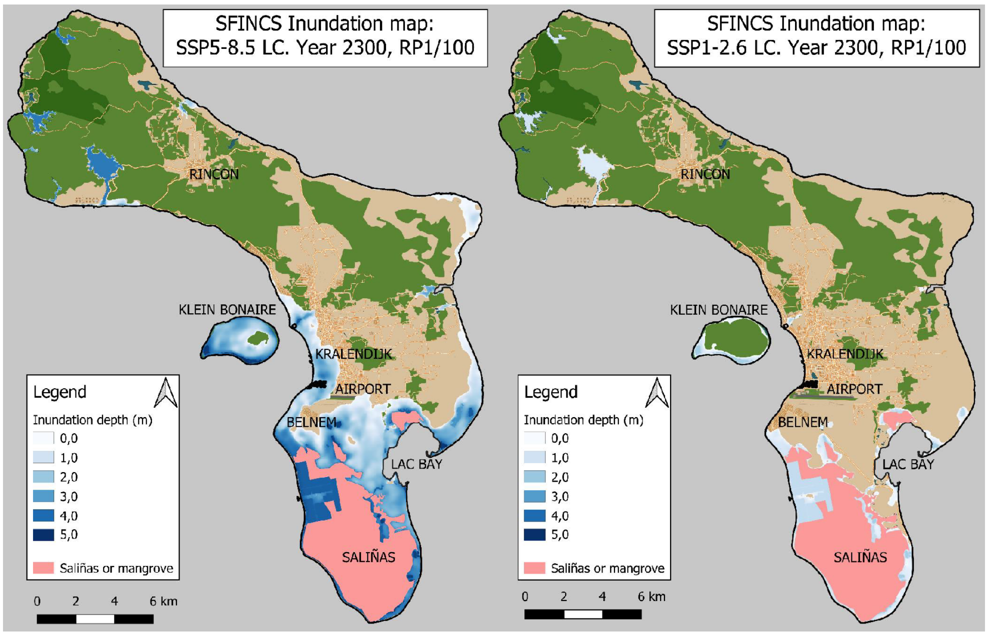
SFINCS Inundation map:
SSP5-8.5 LC. Year 2300, RP1/100
RINCON
KLEIN BONAIRE
KRALENDIJK
AIRPORT
BELNEM
LAC BAY
SALIÑAS
Legend
Inundation depth (m)
0,0
1,0
2,0
3,0
4,0
5,0
Saliñas or mangrove
0 2 4 6 km
SFINCS Inundation map:
SSP1-2.6 LC. Year 2300, RP1/100

Annex G FABDEM validation maps

FABDEM compared to corrected FAMDEM:

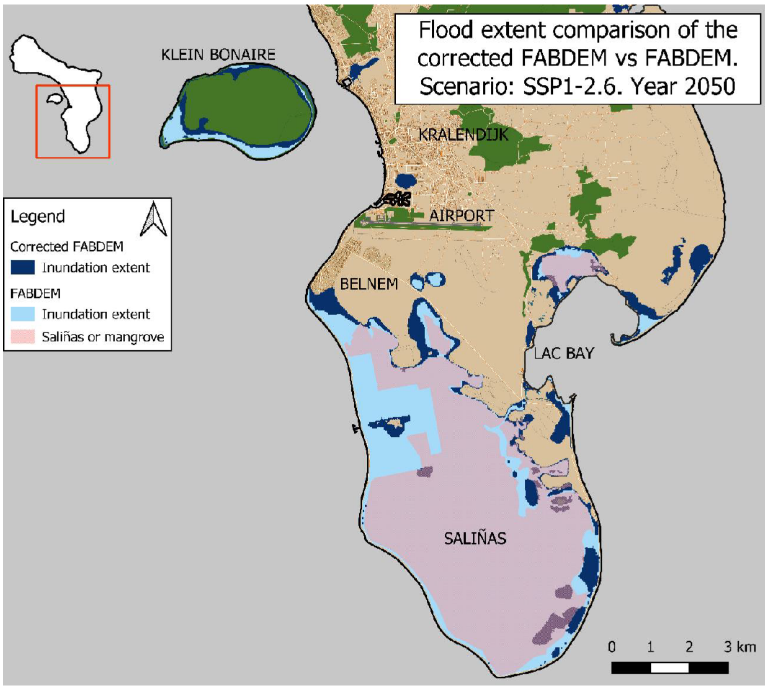

FABDEM compared to CoastalDEM: